Post-Print

Non-modal analysis of coaxial jets

D. Montagnani, F. Auteri†

Dipartimento di Scienze e Tecnologie Aerospaziali, Politecnico di Milano, via La Masa 34, 20156 Milano, Italy

In this work, we investigate the subcritical behaviour of a coaxial jet subject to small-amplitude perturbations at the inflow. We use the results of optimal harmonic analysis and dynamic-mode decomposition (DMD) of the flow fields at a Reynolds number, based on the diameter and maximum velocity of the inner inlet pipe, Re = 200, to show that, for a sufficiently low value of the Reynolds number, the coherent structures appearing in the perturbed dynamics of the nonlinear system can be effectively described in terms of the harmonic response of the flow. We also show that, for larger subcritical values of the Reynolds number, Re = 400, a huge amplification of disturbances quickly makes nonlinear effects relevant. Large-scale, near-field coherent dynamics can be still interpreted as an evidence of the preferred response of the system, using DMD of the flow to describe the noise-driven transition to turbulence downstream. The influence of the axial velocity ratio and the rotational motion of the outer stream is assessed as well. Harmonic analysis successfully predicts the prevalence of rotating helical structures observed in the columnar flow for moderate swirl of the outer jet. Finally, we compare the receptivity of the nonlinear system to the optimal linear perturbations with its response to stochastic forcing. Optimal forcing is still more effective than white noise in driving the system to a turbulent state, where nonlinear dynamics prevail. We still conclude that linear optimal forcing may be relevant in investigating the transition to turbulence in coaxial jets, even if more about the transition process could be learnt from a more expensive nonlinear analysis.

Key words:

1. Introduction

Coaxial jets are employed in several industrial applications, such as in noise control, mixing processes and energy conversion by combustion. Atomizers, burners and mixers exploit the interpenetration of the two streams as an effective mixing mechanism, since the external jet can destabilise the internal jet and, as a consequence, increase mixing by promoting transition to turbulence, see (Villermaux & Rehab 2000) and the references therein. Several aeronautical applications use coaxial jets to reduce the noise produced by the single jet layout (Williams *et al.* 1969). Swirling jets are often employed in combustors to enhance the stability of flame anchoring thus improving the efficiency of the combustion and reducing the NO_x emissions (Lefebvre 1998).

Coaxial jets are also interesting to investigate the subcritical transition process in parallel or quasi-parallel flows. Indeed jets, and in particular coaxial jets, exhibit subcritical transition such as the Couette and Poiseuille flows and boundary layers. With respect to

the abovementioned flows, this phenomenon is particularly notable in coaxial jets that exhibit a very strong nonnormal behaviour (Canton *et al.* 2017). This property makes them ideal for mixing (Schumaker & Driscoll 2012), especially for low Reynolds number applications (Saiki *et al.* 2011).

The mixing and noise-generation properties of coaxial jets are strongly related to their stability since the flow behaviour depends on the dynamics of large-scale coherent vortical structures produced by the amplification of external perturbations. Jets, and coaxial jets in particular, are known to be convectively unstable (Chomaz 2005), with large amplification rates (Garnaud *et al.* 2013*a,b*; Canton *et al.* 2017). The instability modes are usually referred to as *varicose*, when the unstable perturbation is axisymmetric, *sinuous*, when the perturbation appears as a sinusoidal transverse wave propagating along the jet axis and they have azimuthal wavenumber $|m| = 1$, *helical*, when the perturbation resembles a helix with wavenumber $|m| > 1$. When swirl is present in the jet, helical modes are usually characterised by a spiral motion. This motion is termed co-winding, if the helix winds in the same direction of the rotation of the jet, otherwise they are termed counter-winding or retrograde. Several studies in the past have investigated the linear stability of jets in the incompressible and compressible regimes. The inviscid stability of parallel jets was investigated by Batchelor & Gill (1962). They found a sinuous unstable perturbation with $m = 1$ for a top-hat velocity profile, for which the velocity is constant in the central region and then goes rapidly to zero, but noticed a high impact of the velocity profile on the stability properties of the flow. Crighton & Gaster (1976) emphasized the importance of nonparallel effects and of the nozzle region. These effects were fully taken into account by Garnaud *et al.* (2013*a*) and Garnaud *et al.* (2013*b*) who showed the inadequacy of a modal stability analysis to understand the stability of the flow, while pointing out the importance of convective instability.

The swirling jet has been investigated theoretically and numerically exploiting different baseflows: the Batchelor vortex (Leibovich & Stewartson 1983; Khorrami 1991; Delbende & Rossi 2005), a standard or screened Rankine vortex (Loiseleux *et al.* 1998; Gallaire & Chomaz 2003*a*) or other flows (Martin & Meiburg 1994, 1996; Loiseleux *et al.* 2000; Gallaire & Chomaz 2003*b*). The reported results show that instabilities are mainly convective, related to the Kelvin–Helmholtz and centrifugal mechanisms. A stability criterion for the centrifugal instability has been formulated for vortices by Leibovich & Stewartson (1983), then extended by Billant & Gallaire (2013) to swirling-jet flows.

Most of the experimental activity on swirling round jets has been carried out for moderate to high Reynolds numbers, see (Örlü & Alfredsson 2008) and the references therein. More relevant to the present work are experiments in the low Reynolds number range. Loiseleux & Chomaz (2003) considered two different Reynolds numbers, 740 and 1490. For low swirl, the flow behaviour is similar to that observed for a non-swirling jet, namely it is dominated by axisymmetric perturbations whose nonlinear evolution first leads to vortex roll up and then to vortex pairing. A successive instability of the braid connecting to successive vortices, similar to that observed for an axisymmetric jet but featuring corotating vortices, rapidly leads to turbulence. For higher swirl numbers in the range $(0.6, 1)$, the flow is dominated by the wavenumber $m = +2$. For $1 \leqslant S_{\mathrm{LC}} \leqslant 1.3$, strong interaction between the axisymmetric mode and the $m = +2$ mode is observed, leading to the emergence of the $m = +1$ mode. Vortex breakdown is observed for $S_{\mathrm{LC}} \geqslant 1.3$. Experiments carried out by Liang & Maxworthy (2005) for a Reynolds number $\mathrm{Re} = 1000$ showed two different regimes before vortex breakdown. Results similar to those by Loiseleux & Chomaz (2003) are reported in the low swirl regime. In contrast, for intermediate swirl $S_{\mathrm{LM}} \gtrsim 0.6$, the initial part of the flow is dominated by helical modes with wavenumbers $m = +2$ and $m = +3$. For swirl numbers higher than $0.83 \div 0.86$ vortex

breakdown was observed. We note in passing that the definition of swirl number S_{LC} and S_{LM} in the two works is different and different from the definition adopted here, so that the thresholds are not directly comparable.

The theoretical investigation of the stability properties of coaxial jets is more recent. With respect to the round jet, coaxial jets are characterised by several independent parameters, the outer-to-inner ratio R_D, the non-dimensional thickness s of the wall separating the two incoming flows, the Reynolds number Re, the ratio between the maximum axial component of the velocity of the outer and inner jets r_u, the swirl numbers of the inner and outer jet. Michalke (1999) first analysed the inviscid spatio-temporal stability of a parallel annular jet, with possible backflow in the jet core. He found that an absolute instability can arise only for the perturbation with azimuthal wavenumber $m = +1$. If a backflow is present, the absolute instability occurs with or without swirl, while a swirl is necessary if there is no backflow. Talamelli & Gavarini (2006) considered the inviscid linear stability analysis of incompressible coaxial jets mimicking the presence of a blunt wall separating the two jets by a low speed wake in the velocity profile. They found an absolute instability limited to negative or small positive values of the minimum velocity imposed in the wake. They also found that the amplification factor grows as the shear layers thin out. Their findings were substantially confirmed by a global stability analysis by Canton *et al.* (2017) showing that the flow is absolutely unstable for Reynolds numbers above 1356 when a blunt separating wall is present. Canton *et al.* (2017) also showed that the subcritical base flow is convectively unstable with huge amplification of the initial perturbations. Weller-Calvo *et al.* (2015) extended the analysis carried out by Talamelli & Gavarini (2006) to account for a swirl motion.

An extensive experimental activity has investigated coaxial jets. Several works investigated the fully turbulent coaxial jets both without (Champagne & Wygnanski 1971; Buresti *et al.* 1994; Sadr & Klewicki 2003) and with swirl (Ribeiro & Whitelaw 1980; Champagne & Kromat 2000), reporting mainly the mean flow properties and turbulence statistics. More germane to the present investigation are experiments carried out for low and moderate Reynolds number, where details of the instability and transition process are available. In their experiments, Dahm *et al.* (1992) investigated non-swirling jets for three moderate Reynolds numbers (1333, 5867, 10668). For small velocity ratios they observed a sinuous instability with wavenumber $m = \pm 1$ while for $r_u \geqslant 0.71$ they observed the development of an axisymmetric instability. For the higher velocity ratio tested, $r_u = 1.14$, they observed lock in of the perturbations in the outer and inner shear layers. This phenomenon was observed also by Tang & Ko (1994) for Re = 1700 and $r_u = 3.33$. The results presented by Wicker & Eaton (1994) show a different behaviour. For low velocity ratios, $r_u \leqslant 0.71$, they observed the development of axisymmetric structures, before further instabilities break the symmetry, while for $r_u = 1.23$ and 1.45 they observed a helical instability developing in the central jet. When forcing is applied, only axisymmetric vortex rings are produced, with a peak in the response for a Strouhal number St = 0.5. Rehab *et al.* (1997) observed that a recirculation region forms for velocity ratios higher that approximately 8. For lower velocity ratios, but still quite high with respect to those investigated here, they found the outer shear layer dominating the instability process. An important appreciation of the role of the velocity ratio was provided by Segalini & Talamelli (2011), who found three different behaviours: for low velocity ratio, the frequency of the instability depends on the velocity of the internal jet, for high velocity ratios it depends on the velocity of the external jet, while for intermediate velocity ratios it depends on both.

The transition process in incompressible coaxial jets without swirl has been investigated also numerically by da Silva *et al.* (2003); Balarac & Métais (2005); Balarac *et al.*

(2007) without and with external forcing. In particular, they found that the thickness of the boundary layer at the nozzle exit has a strong influence on the instability process. As one may expect, the thinner the boundary layer the stronger the instability. For low velocity ratios they found the initial instability dominated by a sinuous perturbation with wavenumber 1. A secondary instability is found where longitudinal vortices are formed in the braid between successive primary vortices that rapidly leads to transition. A linear spreading of the jet is observed after transition. When axisymmetric forcing is applied, strong axisymmetric vortices are formed. Azimuthal excitation leads to the appearance of relatively short wavelengths undulations in the main vortices whose wavenumber is selected by forcing (Balarac *et al.* 2007).

To clarify the instability mechanisms that eventually lead to transition in coaxial jets, even without an absolute instability, and in particular to assess the role that inflow perturbations play in this process, in this work, we investigate the harmonic response of non-swirling coaxial jets in a region of the space of parameters $Re - r_u$ where the system is globally stable. Then the influence of the swirl parameter S of the outer stream is assessed on the columnar state of coaxial jets with unitary velocity ratio. The base flow is assumed axisymmetric and the homogeneity of the azimuthal coordinate θ allows us to exploit the Fourier decomposition of the perturbation fields to obtain the linear dynamics of the system as a combination of the independent evolution of the modes associated with different azimuthal wave numbers, without resorting to time-stepping techniques. With respect to Canton *et al.* (2017), we adopt a different perspective. Firstly, we analyse the response of the system to inflow disturbances, since this is probably one of the most likely ways disturbances enter the flow field. Moreover, as shown by Garnaud *et al.* (2013*b*), the responses of the flow to optimal inlet forcing and optimal volume forcing are qualitatively very similar at the same frequency. Secondly, we restrict our analysis to lower subcritical Reynolds numbers, to avoid the huge amplifications observed for Reynolds numbers as low as 1000. Thirdly, we analyse the response of the base flow to both axisymmetric and nonsymmetric forcing. Fourth, the effect of swirl is here considered for the first time. Three-dimensional nonlinear simulations with perturbed inflow conditions are also performed in order to verify the validity of the assumptions made, to verify the results obtained and the predominance of the preferred response. Both Dynamic Mode Decomposition and Fourier decomposition of time snapshots are used to describe the global dynamics of the system and to compare the structures emerging in the nonlinear system with the prediction of the linear non-modal analysis.

The paper is organised as follows. The flow configuration is presented in §2. The non-modal harmonic response is recalled, and the numerical approach is described in §3. The influence of the velocity ratio r_u and the swirl parameter S on the base flow and on the harmonic response of axisymmetric base flow is presented in §4 and §5, respectively. The results of fully three-dimensional perturbed direct numerical simulations are presented in §6. Conclusions are drawn in §7.

2. Flow configuration

The incompressible flow produced by two cylindrical coaxial jets is considered here. The reference length is chosen as the diameter $\widetilde{D}_i$ of the inner pipe and the reference velocity as the maximum of the inner axial velocity profile, $\widetilde{U}_a$. A slice of the numerical domain is depicted in figure 1. The outer-to-inner ratio of the pipe diameters is $R_D = 2.0$, the non-dimensional thickness of the septum is $s = 0.1$. The length of the inlet pipes is set to $\ell_{in} = 2.5$. The length and the radius of the numerical domain are set to $L_c = 60.0$ and $R_c = 8.0$ (Canton *et al.* 2017). The Reynolds number is defined as $Re = \widetilde{U}_a \widetilde{D}_i / \widetilde{\nu}$,
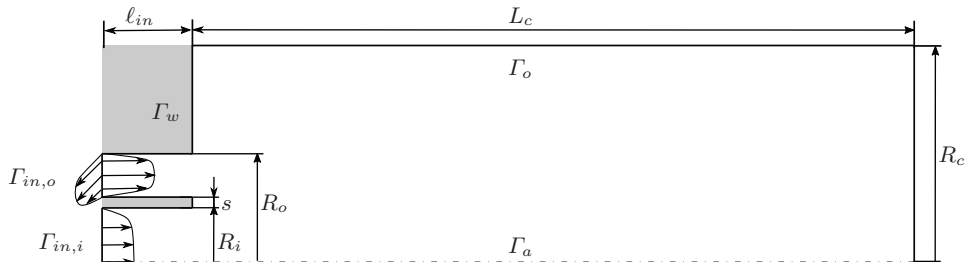
Figure 1: Azimuthal slice of the three-dimensional axisymmetric domain, coinciding with the numerical domain used for the response analysis of the axisymmetric base flow. Figure not drawn to scale.

where $\widetilde{\nu}$ is the constant kinematic viscosity of the fluid. The dynamics of the flow is governed by the non-dimensional incompressible Navier-Stokes equations

$$\begin{cases} \dfrac{\partial \boldsymbol{U}}{\partial t} + (\boldsymbol{U} \cdot \boldsymbol{\nabla})\,\boldsymbol{U} - \mathrm{Re}^{-1}\varDelta \boldsymbol{U} + \boldsymbol{\nabla}P = \boldsymbol{0}, \\[2mm] \boldsymbol{\nabla} \cdot \boldsymbol{U} = 0, \end{cases} \tag{2.1}$$

where $\boldsymbol{U} = \boldsymbol{U}(\boldsymbol{r}, t)$ denotes the nondimensional velocity field, and $P = P(\boldsymbol{r}, t)$ the nondimensional reduced pressure field. A no-slip condition is imposed on the wall boundary $\varGamma_w$, while a homogeneous Neumann condition is assumed on $\varGamma_o$, $\mathrm{Re}^{-1}\hat{\boldsymbol{n}} \cdot \boldsymbol{\nabla}\boldsymbol{U} - P\hat{\boldsymbol{n}} = \boldsymbol{0}$. Axisymmetry conditions, $U_r = 0, U_\theta = 0, \partial U_r/\partial z = 0$, hold on the axis. On the inner and outer inlet boundaries, $\varGamma_{in,i}$ and $\varGamma_{in,o}$ respectively, the axial velocity component is set according to the expressions $U_{z,i}(r)$ and $U_{z,o}(r)$ used by Canton *et al.* (2017) to reproduce the mean *axial* velocity profiles measured by Segalini & Talamelli (2011). The azimuthal velocity profile $U_{\theta,o}(r) = S\,U_{z,o}(r)$ at the inflow boundary of the outer jet $\varGamma_{in,o}$ is chosen proportional to the axial profile $U_{z,o}$ to have a swirl number S, defined as the ratio of these two velocity components, independent of the radius. This definition differs from that mainly used in the literature for the single jet, see for instance (Liang & Maxworthy 2005), and also from that adopted by Gallaire & Chomaz (2003b), owing to the difference in the flows.

$$\boldsymbol{U}\big|_{\varGamma_{in,i}} = U_{z,i}(r)\hat{\boldsymbol{z}}, \tag{2.2}$$

$$\boldsymbol{U}\big|_{\varGamma_{in,o}} = r_u U_{z,o}(r)\hat{\boldsymbol{z}} + r_u U_{\theta,o}(r)\hat{\boldsymbol{\theta}}, \tag{2.3}$$

with

$$U_{z,i}(r) = \tanh\left[b_i\left(1 - 2r\right)\right], \tag{2.4a}$$

$$U_{z,o}(r) = \tanh\left[b_o\left(1 - \left|\frac{2r - (R_{o,1} + R_{o,2})}{R_{o,1} - R_{o,2}}\right|\right)\right], \tag{2.4b}$$

where $R_{o,1}$ and $R_{o,2}$ are the internal and external radii of the annular duct and the two parameters b_i and b_o control the thickness of the boundary layers: both values are set to 5.0 as previously done by Canton *et al.* (2017).

3. Mathematical formulation

The amplification of a small-amplitude stochastic forcing $\boldsymbol{f}$, whose evolution is governed by the linearised system $\boldsymbol{u} = \mathcal{R}\boldsymbol{f}$, can be obtained as a function of the harmonic response of the system, over the whole spectrum of frequencies (Farrell & Ioannou 1996). Boujo & Gallaire (2015) expressed the ensemble variance

$$E = \frac{1}{2\pi} \int\limits_{-\infty}^{+\infty} \sum_k G_k^2(\omega)d\omega = \frac{1}{\pi} \int\limits_0^{+\infty} \sum_k G_k^2(\omega)d\omega \tag{3.1}$$

as a function of the optimal and suboptimal harmonic gains G_k, defined either as the singular values of the linearised Navier–Stokes operator $\mathcal{R}$ or the square root of the eigenvalues of the Hermitian operator $\mathcal{R}^\dagger \mathcal{R}$.

The harmonic response of the flow to velocity perturbations at the inflow is investigated by a non-modal analysis of the linearised flow around the steady axisymmetric solution of the Navier–Stokes equations (2.1). Both axisymmetric and non-axisymmetric perturbations are investigated. The continuity of the fields implies that perturbations must be 2π-periodic in θ and therefore they can be effectively represented by their Fourier series

$$(\boldsymbol{u}, p)(r, \theta, z, t) = \boldsymbol{q}(r, \theta, z, t) = \sum_{m=-\infty}^{\infty} \boldsymbol{q}_m(r, z, t)e^{im\theta}. \tag{3.2}$$

Since the perturbation $\boldsymbol{q}(\boldsymbol{r}, t)$ is real, the complex-conjugate symmetry $\boldsymbol{q}_{-m} = \boldsymbol{q}_m^*$ holds for the series coefficients. The harmonic response of the system to small-amplitude perturbations is described in the frequency domain by the Fourier transform of the linearised Navier–Stokes equations

$$\begin{cases} i\omega\hat{\boldsymbol{u}} + (\boldsymbol{U} \cdot \boldsymbol{\nabla})\hat{\boldsymbol{u}} + (\hat{\boldsymbol{u}} \cdot \boldsymbol{\nabla})\boldsymbol{U} - \mathrm{Re}^{-1}\Delta\hat{\boldsymbol{u}} + \boldsymbol{\nabla}\hat{p} = \boldsymbol{0}, \\ \boldsymbol{\nabla} \cdot \hat{\boldsymbol{u}} = 0, \end{cases} \tag{3.3}$$

supplied with homogeneous Dirichlet and Neumann boundary conditions on Γ_w and Γ_o, respectively, and wavenumber-dependent symmetry conditions on the axis. The harmonic forcing at the inflow is introduced as the essential boundary condition $\hat{\boldsymbol{u}} = \hat{\boldsymbol{f}}$ on Γ_i. By the linearity of this model, with reference to the series (3.2), the dynamics of the system is obtained as a combination of the independent evolution of the modes with different wave numbers, governed by the complex equations

$$\begin{cases} i\omega\hat{\boldsymbol{u}}_m + (\boldsymbol{U} \cdot \boldsymbol{\nabla}_m)\hat{\boldsymbol{u}}_m + (\hat{\boldsymbol{u}}_m \cdot \boldsymbol{\nabla}_0)\boldsymbol{U} - \mathrm{Re}^{-1}\Delta_m\hat{\boldsymbol{u}}_m + \boldsymbol{\nabla}_m\hat{p}_m = \boldsymbol{0}, \\ \boldsymbol{\nabla}_m \cdot \hat{\boldsymbol{u}}_m = 0, \end{cases} \tag{3.4}$$

where $(\hat{\boldsymbol{u}}_m, \hat{p}_m)(\boldsymbol{r}, \omega)$ indicates the contribution of the m-th wavenumber $(\boldsymbol{u}_m, p_m)(\boldsymbol{r}, t)$ to the perturbation field and the complex operators $\boldsymbol{\nabla}_m$, Δ_m for axisymmetric fields are obtained by formally replacing the partial derivative $\partial/\partial\theta$ in the original equations with the factor im in the transformed equations. The phase velocity of a perturbation with wavenumber m and frequency ω is obtained as $\Omega_m = -\omega/m$ by explicitly writing the inverse Fourier transform

$$\boldsymbol{q}(\boldsymbol{r}, t) = \frac{1}{2\pi} \int_{-\infty}^{\infty} \hat{\boldsymbol{q}}_m(r, z, \omega)e^{i(m\theta + \omega t)}. \tag{3.5}$$

The harmonic response of the axisymmetric base flow is computed with a finite element solver of the Navier–Stokes equations in cylindrical coordinates, developed starting from the well-validated baseline code resulting from a collaboration between Politecnico di
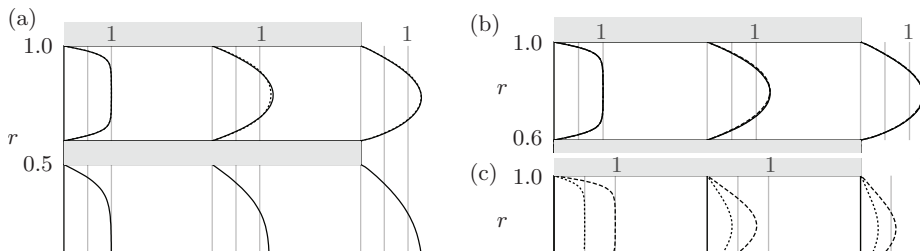
Figure 2: Velocity profile in the inlet pipes. (a) Axial velocity for Re = 200, $S = 0$: $r_u = 1.0$ (solid line), $r_u = 2.0$ (dashed line). In the outer pipe, the velocity is normalised with the maximum value of the axial velocity at the inflow. Axial (b) and azimuthal (c) velocity in the outer pipe for Re = 200, $r_u = 1.0$: $S = 0.5$ (dotted line), $S = 1.0$ (dashed line).

Milano and KTH (Canton *et al.* 2017). The discrete form of the fields and the weak formulation of the problem is built on the standard Taylor–Hood $\mathbb{P}_2$–$\mathbb{P}_1$ finite elements of an unstructured triangulation (Dussin *et al.* 2009) of the numerical domain corresponding to an azimuthal slice of the actual domain. The details of the grid are given in appendix A. The axisymmetric flow is computed by Newton's iteration, while the computation of the harmonic response follows Garnaud *et al.* (2013*b*). The spectral element code Nek5000 is used for three-dimensional direct numerical simulations. This is a massively parallel, open-source code based on a spatial discretisation by hexahedral spectral elements with Lagrangian tensor-product bases built on Gauss–Legendre–Lobatto points. A second-order fractional step method is used to advance the solution in time, with a BDF2 implicit treatment of the viscous term and a consistent explicit treatment of the nonlinear term in the momentum equation (Fischer *et al.* 2008). The compatible formulation $\mathbb{P}_N$–$\mathbb{P}_{N-2}$ is used for the velocity and pressure fields, with $N = 7$. The initial condition coincides with the axisymmetric base flow used for the harmonic response. Dynamic mode decomposition (Schmid 2010) is used to describe the global behaviour of the perturbed systems by means of Koopman mode analysis.

4. Base flow

The base flow is briefly described as a function of the outer-to-inner axial velocity ratio r_u and of the swirl parameter S. As observed by Canton *et al.* (2017), the inlet axial velocity profile, that mimics the mean velocity measured by Segalini & Talamelli (2011) at higher Reynolds number, is gradually smeared along the inlet pipe, due to the higher impact of viscous effects at this lower Reynolds number. The thickness of the boundary layer grows along the pipe and the axial velocity profiles qualitatively approach fully developed profiles with the maximum of the axial velocity profile that increases, as shown in figure 2(a) and (b). The axial velocity profile, normalised with respect to the velocity ratio r_u, is almost independent of this parameter, as shown in figure 2(b) by superimposing the normalised velocity profiles U_z/r_u corresponding to different values of r_u. The shape of the azimuthal velocity profile changes along the outer pipe, while its maximum value decreases, due to viscous dissipation, as shown in figure 2(c) for Re = 200 and $r_u = 1.0$.

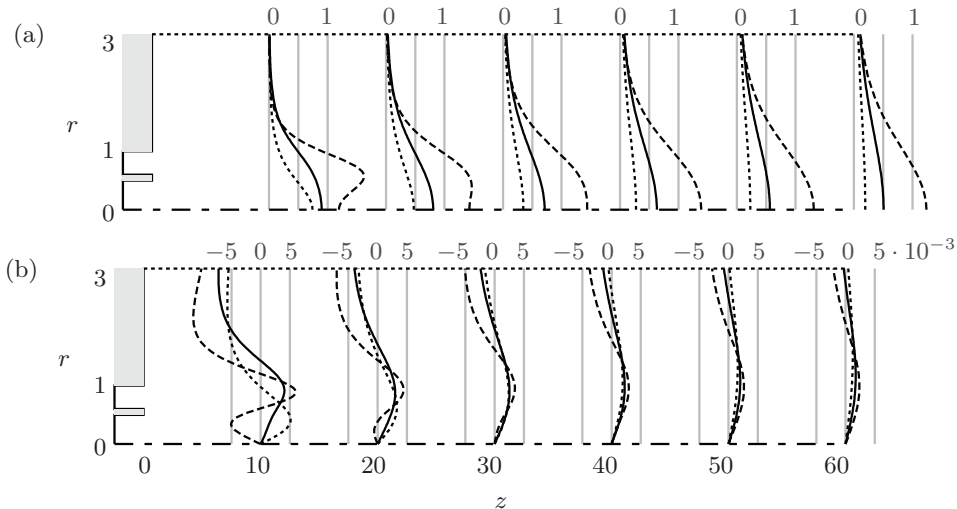The velocity profiles of the non-swirling jets are depicted in figure 3 for several distances

Figure 3: Influence of the velocity ratio r_u on the (a) axial and (b) radial velocity fields in the domain. Non-swirling jet for Re $= 200$, $r_u = 0.0$ (dotted line), $r_u = 1.0$ (solid line) and $r_u = 2.0$ (dashed line).

r_u	$z = 10$	$z = 20$	$z = 30$	$z = 40$	$z = 50$	$z = 60$
0.0	3.23	4.59	5.35	5.68	5.73	5.61
1.0	1.89	2.32	2.57	2.72	2.81	2.86
2.0	1.66	2.04	2.32	2.52	2.68	2.79

Table 1: Entrainment in stable non-swirling base flows. Ratio of the mass flow $Q(z) = 2\pi \int_{r=0}^{R=3} U_z(r,z)r dr$ through circular surfaces orthogonal to the axis, and the mass flow at the inflow, $Q_{in} = Q_{in,i} + r_u Q_{in,o} = 0.593 + 1.732\, r_u$. Re $= 200$.

from the orifice and for different values of the velocity ratio r_u. In these non-swirling cases, the azimuthal component of the velocity is zero for symmetry. No recirculation bubble has been observed downstream of the septum separating the inlet ducts, for the values of the parameters under investigation. For velocity ratios lower than $r_u = 1.0$, the maximum axial velocity is attained on the axis and no other local maxima associated with the outer stream are observed for $z \geqslant 10$. In this case, a single shear layer characterises the flow field in the region far from the nozzle, while three different shear layers are always present near the nozzle owing to the presence of the blunt wall separating the inner and outer jet. For $r_u = 2.0$, a local maximum is attained in the domain for $z \geqslant 10$ and a local minimum is observed on the axis for $z \leqslant 20$. This behaviour of the axial velocity for high velocity ratios is associated with a non-trivial radial velocity profile, as shown in figure 3(b). For low velocity ratios, the positive values of U_r near the axis and the negative values far from the axis are associated with the spreading of the jet core and the entrainment process, respectively. For $r_u = 2.0$, as the maximum of the axial velocity moves from the outer stream towards the axis for $z < 20$, a negative radial velocity is observed near the axis. Such a negative radial velocity is related, by incompressibility, to
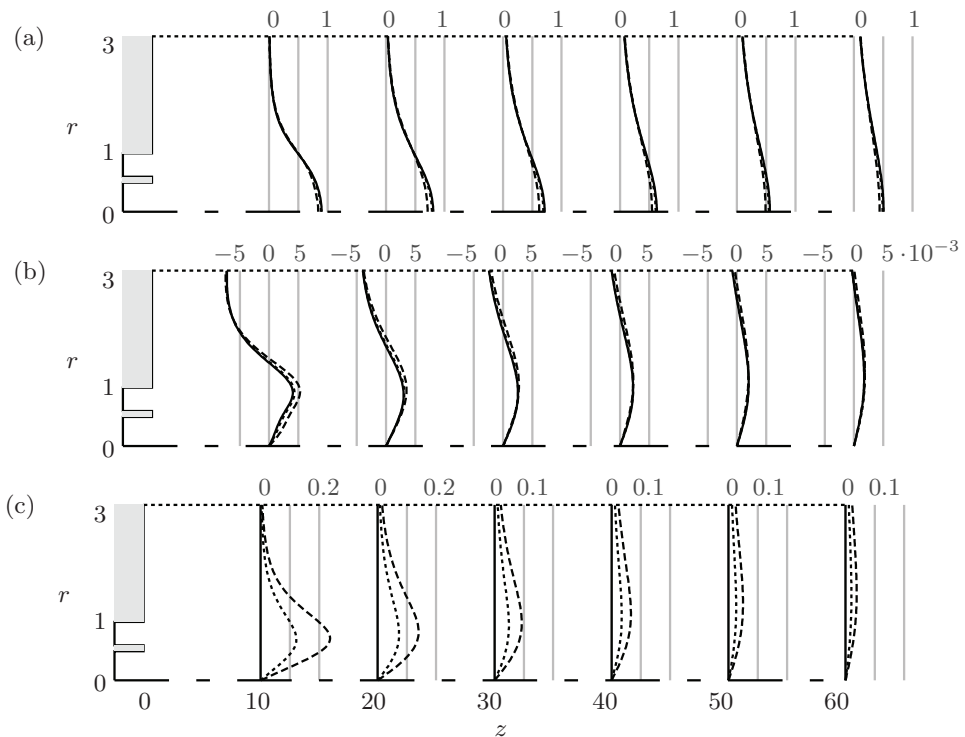
Figure 4: Influence of the swirl ratio S of the outer stream on the (a) axial, (b) radial and (c) azimuthal velocity fields in the domain. Swirling jet for Re = 200 and $r_u = 1.0$: $S = 0.0$ (solid line), $S = 0.5$ (dotted line) and $S = 1.0$ (dashed line).

the transfer of momentum from the high-speed region of the jet to the near axis region, and in fact is no longer observed when the maximum of the axial velocity eventually reaches the axis.

The velocity field in the domain for jets with unitary velocity ratio and different values of the swirl parameter is depicted in figure 4. As it is clear from the figure, the longitudinal and radial velocity components of the base flow are quite insensitive to the swirl, for small swirl ratios. Despite this fact, as it will be appreciated later on, this parameter can impact the response of the flow to inflow perturbations quite dramatically.

5. Harmonic response

Despite this flow is absolutely stable, according to a global modal stability analysis Canton *et al.* (2017), transition to turbulence in jets has been observed for Reynolds numbers well below Re = 500 (Reynolds 1962). In fact, modal stability does not tell us the whole story, since nonnormal systems, such as jets, may exhibit transient growth and pseudo-resonance (Reddy & Henningson 1993; Schmid 2007), i.e. a large amplification of initial perturbations and external forcing in a restricted range of frequencies due to nonmodal growth mechanisms. Such an amplification of perturbations, that are always present to a certain degree in an experiment, may lead to secondary instabilities and eventually to turbulence (Blackburn *et al.* 2008a,b; Cantwell *et al.* 2010). The transient

growth of axisymmetric perturbations has been already analysed by Canton *et al.* (2017), that found huge amplification factors for a subcritical Reynolds number of 1000, while the harmonic response has been investigated for the single jet by Garnaud *et al.* (2013*b*) for the same Reynolds number. In this section, the harmonic response of the coaxial-jet flow to small-amplitude inflow forcing is investigated to explain the preferred dynamics of the system observed experimentally (Dahm *et al.* 1992) or by direct numerical simulations with forcing applied at the inlet (Balarac *et al.* 2007). The nonlinear response of the flow to inflow forcing is also investigated in §6 by direct numerical simulation to investigate the relevance of the linear response when nonlinearities are present. A Reynolds number lower than that employed in (Canton *et al.* 2017; Garnaud *et al.* 2013*b*) has been preferred here to avoid the huge amplifications observed for Reynolds numbers of the order of 1000 and therefore to better appreciate the spatial evolution of perturbations.

5.1. *Non-swirling jet*

Firstly, the effect of the velocity ratio r_u on the harmonic response of non-swirling jets with Re = 200 is investigated. The relative contributions $g_k(\omega) = G_k(\omega)/\max_{i,\omega}\{G_i(\omega)\}$ of the optimal and suboptimal responses associated with different wavenumbers are represented in figure 5(a-c) as functions of the frequency of the harmonic perturbations, for different values of the velocity ratio r_u. The shape of the optimal responses is depicted in figure 5(d-f). The optimal sinuous and varicose responses, with azimuthal wavenumbers $m = +1$ and $m = 0$, respectively, prevail over the response to forcing with larger wavenumbers, so that results only for these two wavenumbers are reported in figure 7. For instance, the harmonic gain of the optimal sinuous response of the single jet is approximately three times larger than the optimal axisymmetric gain. Dominant perturbations with $m = 0$ and $m = +1$ were found also by Mattingly & Chang (1974), by an inviscid local linear stability analysis of the round jet, but in that case the $m = 0$ perturbation was found to be more amplified. This result is similar to what has been found for the single jet by Morris (1976), see also (Danaila *et al.* 1997). The varicose and sinuous modes emerge as dominant for different velocity ratios also in coaxial jets. It is interesting to note that Wicker & Eaton (1994) found that varicose and sinuous large-scale coherent structures are still dominating the flow behaviour at Reynolds numbers orders of magnitude higher. For low values of the velocity ratio, a local maximum appears on the axisymmetric optimal response, while both the frequency and the shape of the preferred axisymmetric response undergo substantial changes in the range of velocity ratio $r_u \in (0.5, 1.0)$, as shown in figure 5(b-c,e-f). A second local maximum appears in the optimal harmonic response at $\omega = 0.67$, it becomes the global maximum as the velocity ratio exceeds $r_u = 0.75$, while the low-frequency maximum disappears for larger values of r_u, see figure 6.

The optimal harmonic gain and the frequency of the pseudo-resonance peaks for $m = 0$ and $m = +1$ are shown in figure 7(a) and (b), respectively, as functions of the velocity ratio r_u. Two different regions can be distinguished in the two plots. For small velocity ratios, $r_u \lesssim 0.5$, the maximum harmonic gain and its frequency are almost insensitive to r_u. We conjecture that in this case the flow behaviour is dominated by the inner jet as in (Segalini & Talamelli 2011), or more precisely by the shear layer between the inner and outer jet that is rapidly amalgamated with the external shear layer, as visible in figure 2(a). This observation is confirmed by noticing that the shapes of the optimal responses for $r_u = 0$, namely for the single jet, and for $r_u = 0.5$, reported in figure 5(d-e), are very similar and that the optimal response reaches its maximum near the axis for $m = 0$ and in a region that corresponds to the inner shear layer for $m = \pm 1$. For higher velocity ratios, $r_u \gtrsim 1$, the flow behaviour changes. The optimal responses for $m = 0$ and

$m = +1$ have very similar gain. The maximum amplification grows exponentially with the velocity ratio. This is especially evident for $m = \pm 1$, while for $m = 0$ there could be some saturation for $r_u > 2$, figure 7(a). More than one order of magnitude in the peak response amplitude is gained by just doubling the velocity ratio. This result is probably related to the exponential growth of the maximum harmonic gain as a function of the Reynolds number observed by Boujo & Gallaire (2015) for the backward facing step, and that of the maximum transient growth observed by Cantwell *et al.* (2010) for several wall-bounded separated flows. Indeed, in the present case the Reynolds number of the flow is computed as a function of the maximum velocity of the internal jet, but clearly the ratio of inertia terms over viscous terms for the external shear layer grows almost linearly with the velocity ratio r_u when the Reynolds number is fixed. The frequency of the maximum amplification, the pseudo-resonance peak, grows linearly as a function of r_u, figure 7(b), showing that, for sufficiently high velocity ratios, the flow properties scale with the external velocity and the outer jet dominates the stability properties of the flow (Rehab *et al.* 1997). It must be added here that the two preferred dynamics associated with the pseudo-resonance peaks in the harmonic response of the flow at $r_u = 1.0$ persist for higher values of the velocity ratio. The trend observed here, with the ratio of the amplitudes of the axisymmetric and $m = \pm 1$ modes growing with the velocity ratio, has been observed also by Dahm *et al.* (1992). Indeed, they reported the development of a sinuous $m = \pm 1$ mode for $r_u = 0.59$ while an axisymmetric mode is observed for the higher $r_u = 0.71$, both associated with the external shear layer. Interestingly enough, our results show, see figure 7(a), a change in the dominating axisymmetric mode for $r_u = 0.75$. While the total amplification of the axisymmetric mode reaches that of the sinuous mode only for r_u higher than 1, the former is more amplified near the nozzle than the latter, and could be therefore observed experimentally, especially for Reynolds numbers higher than the present ones.

The behaviour observed for the frequency of the optimal response is only partially coherent with the results reported by Segalini & Talamelli (2011) that found three different behaviours as a function of the velocity ratio: for $r_u < 0.75$ the frequency of the main peak in the radial-velocity spectrum scales as the velocity of the internal jet; for $r_u > 1.6$ the frequency scales as the velocity of the external jet. These observations are coherent with the present results. For $0.75 < r_u < 1.6$, however, Segalini & Talamelli (2011) observed that the frequency depends on a combination of both. This behaviour is observed here for $m = \pm 1$. For $m = 0$, the picture is more involved since, as previously observed, two different peaks in the optimal response exchange the role of pseudo-resonance in the interval $0.5 < r_u < 1$. For $r_u < 0.75$, the frequency of the pseudo-resonance peak for $m = 0$ scales as that of the optimal $m = \pm 1$ mode, consistently with Segalini & Talamelli (2011). For $r_u \geqslant 0.75$, the pseudo-resonance peak moves to a higher frequency, and its frequency scales almost as the external velocity, especially for $r_u \geqslant 1$, as shown in figure 7(b). The radical change in the shape of the optimal response as r_u is increased beyond 0.75 is associated with the high-frequency dynamics that becomes dominant in this range of the parameter, as shown in figure 6(b). For low velocity ratios, figure 5 (d) and (e), the optimal response is very elongated in the axial direction, with large structures that are more intense on the axis and slowly decay with z. The axisymmetric structures for both $r_u = 0$ and $r_u = 0.5$ are similar to that found by Garnaud *et al.* (2013b) for the single jet, while the frequencies differ, probably due to the different Reynolds numbers. They presented the spatial structure of the response only for axisymmetric perturbations, so that a comparison is not possible for $m = 1$, but it must be said that they also observed a larger response for $m = 1$ than for $m = 0$. For $r_u = 1$, we observe a totally different shape of the response. First, the response has a

frequency approximately one order of magnitude higher. Moreover, the space distribution of the response has two local maxima: one in the region of the external shear layer and one along a line starting from the wall separating the two jets and reaching the axis after more than ten internal diameters. The response spreads more in the radial direction than for lower velocity ratios. Finally, it is evident that the linear response decays very quickly, being almost negligible 20 diameters downstream the jet exit. This behaviour is similar to what found experimentally by Dahm *et al.* (1992) for $r_u = 1$ and 1.14. They observed a wake-like instability in the shear layers produced by the separating wall frequency locked to the axisymmetric roll-up associated with the external shear layer. The shape of the axisymmetric mode in figure 5(f) seems to represent reasonably well both the instabilities. The change of shape is associated with the higher frequency local maximum in the frequency response becoming dominant over the lower frequency pseudo-resonance peak for $r_u \approx 0.75$, as shown in figure 6(b). The shape of the response is very similar to that reported by Garnaud *et al.* (2013b) for the single jet, even if a local maximum is also found in the present case in the wake of the separating wall. In order to compare the Strouhal numbers, we need to take into account that, for $r_u = 1$, the jet behaves almost as a single jet with nozzle diameter equal to that of the external nozzle of the coaxial jets, and that the Reynolds numbers are different. The present result $\omega = 1$ leads to a Strouhal number based on the diameter of the outer jet and on the maximum velocity of 0.31. This value, once rescaled for Re = 1000 using a linear variation of the frequency with the Reynolds number obtained from results reported later on, agrees very well with the value St = 0.48 reported by Garnaud *et al.* (2013b). The observed trend of the response as a function of the velocity ratio is confirmed by the results reported in figure 8 for a velocity ratio $r_u = 2$. The shape of the optimal response suggests that for high velocity ratios the flow is dominated by the outer shear layer. In this case, the amplification of the axisymmetric mode reaches the value of the sinuous mode with $m = \pm 1$. The shape of the strongest response modes is very similar to that observed for $r_u = 1$, but the maximum of the optimal axisymmetric response moves considerably downstream. The fact that the axisymmetric response dominates in the region near the nozzle agrees with the experimental observations by Rehab *et al.* (1997) for nonrotating coaxial jets with $r_u \geqslant 2$. It is interesting to note that the switch between the low r_u behaviour and the high r_u behaviour is observed for a velocity ratio for which the momentum flux exiting from the inner nozzle approximately equals that exiting from the outer nozzle.

5.2. *Effect of swirl*

The effect of the swirl parameter is assessed for coaxial jets with $r_u = 1$. The rotation of the outer stream breaks the symmetry of the azimuthal coordinate θ, so that retrograde structures have positive wavenumbers in the series expansion (3.2) for positive values of ω. While the amplification of axisymmetric structures remains almost unchanged, huge amplifications of the non-axisymmetric retrograde modes occur in swirling jets, see figure 9(a): the $m = +1$ mode prevails for low swirl, while the contribution of larger wavenumbers emerges as the swirl parameter S exceeds 0.6, see figure 10(a-b). The optimal amplification of structures with wavenumbers 2, 3, 4 grows exponentially fast for $S > 0.5$. The response of the system associated with negative azimuthal wavenumbers corresponding to forward rotation rapidly decays with ω and S, see dotted lines in figure 10(a-c). For $S = 1$, the retrograde structures with wavenumbers $+2$ and $+3$ are dominant (c).

The analysis of the spatial structure of the optimal response is also interesting. For $S = 0.2$, figure 10(d), the optimal response, a single retrograde helix with wavenumber $m = +1$, is mostly amplified quite far from the nozzle. The maximum of the response is
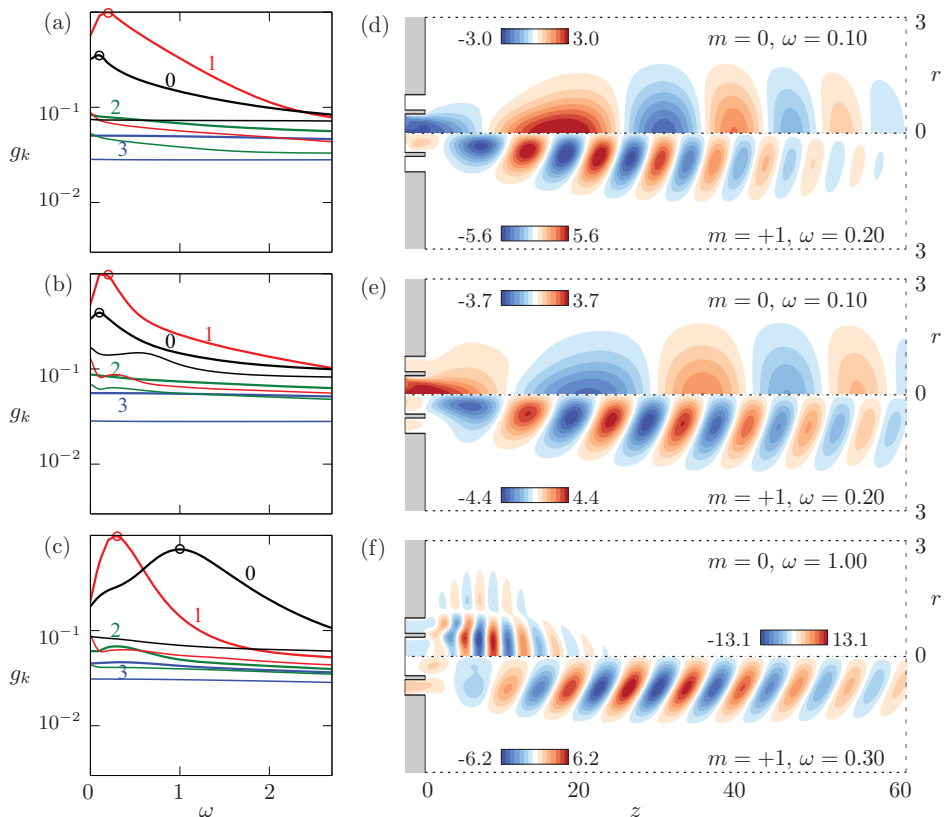
Figure 5: Influence of the velocity ratio r_u on the harmonic response of non-swirling jets for Re = 200. Relative contributions of the wavenumbers in the harmonic response (left) and real part of the axial velocity $\hat{u}_z$ of the preferred response (right): $r_u = 0.0$ (a,d); $r_u = 0.5$ (b,e); $r_u = 1.0$ (c,f). Thick lines in the left plots represent optimal gains, while thin lines represent the first suboptimal gain.

observed for a radius slightly less than one. On this point, it is interesting to observe that Leibovich & Stewartson (1983) predicted that the eigenfunctions should be maximum around $R = 1$, and this property was observed also for the peak of the impulse response of a swirling jet by Gallaire & Chomaz (2003b). As the swirl number is increased, figure 10(b-c), the optimal response is associated with increasing wavenumbers, but the spatial structure of the optimal response does not change dramatically. The maximum of the response moves farther from the nozzle as the swirl number is increased; the opposite trend is observed as the wavenumber is increased. The optimal response associated with these helical structures extends throughout the whole domain. Moreover, it can be observed that the radius where the maximum of the optimal response is observed slowly grows with the swirl number, while remaining always in the neighbourhood of $r = 1$. This effect is probably related to the slow growth of the radius of the jet as the swirl number is increased, see figure 4(a).

Despite the difference in the base flow and Reynolds number, our results seem to qualitatively agree with the experimental results reported by Liang & Maxworthy (2005).
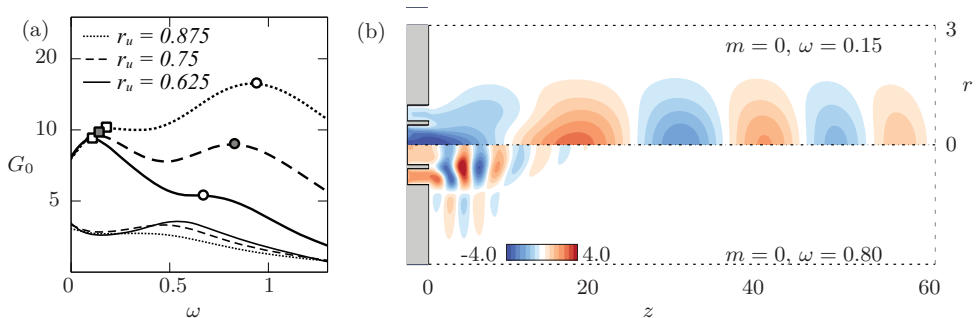
Figure 6: Influence of the velocity ratio $r_u \in (0.625, 0.875)$ on the axisymmetric harmonic response of non-swirling jets for Re = 200. (a) Amplification G_0 of the optimal (thick lines) and first suboptimal (thin lines) axisymmetric harmonic response. Square and circle markers identify the first and the second local maximum, respectively, as in figure 7. (b) Real part of the axial velocity $\hat{u}_z$ of the two preferred axisymmetric responses for $r_u = 0.75$.
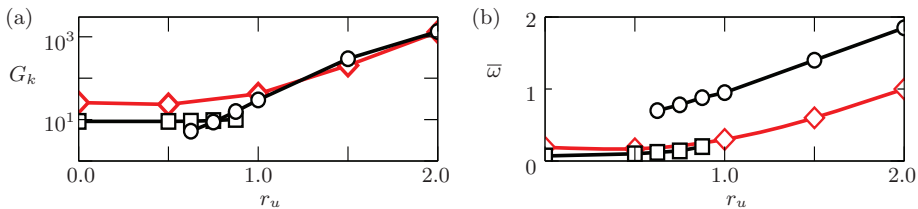

Figure 7: Influence of the velocity ratio r_u on the harmonic response of non-swirling jets for Re = 200. (a) Amplification G_k and (b) frequency $\overline{\omega}$ of the pseudo-resonance peaks. Line colours identify the wavenumbers: $m=0$, black lines; $m=1$, red lines with diamonds. Markers identify the preferred responses: squares and circles represent the first and the second peak of the axisymmetric harmonic gain, respectively.

Indeed, for strongly swirling jets before vortex breakdown, they found an instability in the form of retrograde, i.e. counter-winding, helical waves with $m = +2$ and $m = +3$. For smaller values of the swirl number, the instability is associated with axisymmetric annular vortices, while spiral vortices are associated with a secondary instability. This last observation is not completely in contrast with our results. While for small swirl the axisymmetric mode is globally less amplified than the $m = +1$ helical mode, it is indeed stronger in the region near the nozzle. Therefore, we conjecture that we observe axisymmetric vortices since they are the most amplified ones near the nozzle. Then, a secondary instability sets in before the helical mode is sufficiently amplified to be visible, as will be clearer in the next section. In contrast, our result are different from that reported by Gallaire & Chomaz (2003b) where co-winding modes are most amplified. The main reason to explain this discrepancy probably relies in the different base flow. In the present case, since only the outer jet is swirling, two azimuthal shear layers are present that are at the origin of the observed counter-winding modes. As a confirmation,
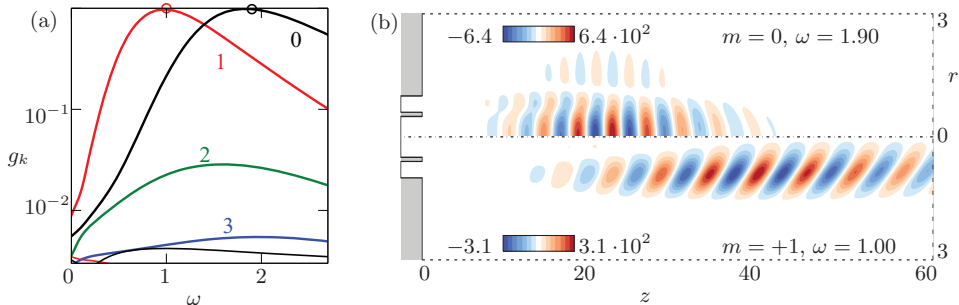
Figure 8: Harmonic response for $(\mathrm{Re}, r_u, S) = (200, 2.0, 0.0)$. (a) Relative contributions of the wavenumbers. Thick lines indicate the optimal harmonic gain, while thin lines the first suboptimal harmonic gain. The small circles on the curves correspond to the preferred response shown in the right frame. (b) Real part of the axial velocity $\hat{u}_z$ of the preferred response.
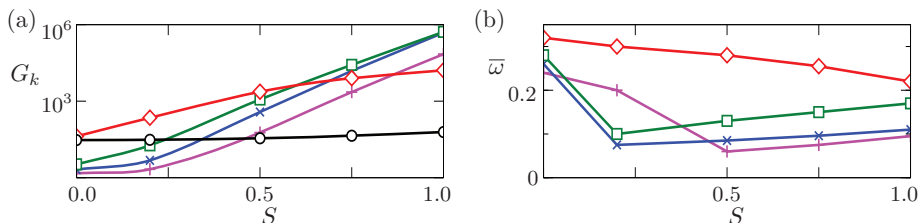

Figure 9: Influence of the swirl parameter S on the harmonic response: coaxial jets with unitary velocity ratio and $\mathrm{Re} = 200$. (a) Optimal amplification G_k and (b) frequency $\overline{\omega}$ of the pseudo-resonance peak. Line colours and markers identify the wavenumbers: $m = 0$ black circles; $m = +1$ red diamonds; $m = +2$ green squares; $m = +3$ blue crosses; $m = +4$ magenta plus markers. The pseudo-resonance peak of the axisymmetric mode is approximately $\overline{\omega}_0 \approx 1$ over the whole range of S explored. Only retrograde dynamics is represented.

we observe that Weller-Calvo *et al.* (2013) did not find such modes by a linear stability analysis of the parallel coaxial-jet flow for $r_u \approx 1$, when only the central jet is swirling.

5.3. *Effect of the Reynolds number*

The influence of the Reynolds number Re on three flow configurations is summarised in figure 11. In general, we can say that the Reynolds number mainly affects the magnitude of the amplification while it has only a minor impact on the frequency of the pseudo-resonance peaks. For the single jet, figure 11(a), two main effects are observed. The amplitude of sinuous response modes with $m = +1$, $m = +2$ and $m = +3$ increases significantly with the Reynolds number. The most amplified response corresponds to $m = \pm 1$. The peak response amplitude of the axisymmetric mode, in contrast, does not change significantly, but a second local maximum appears for a nondimensional circular frequency $\omega \approx 2$. The situation is different when a coaxial jet with unitary velocity ratio is concerned, figure 11(b). In this case, all the responses with lower wavenumber $m = 0 \div 3$ increase significantly. In particular, for the $m = 0$ and $m = +1$ modes the
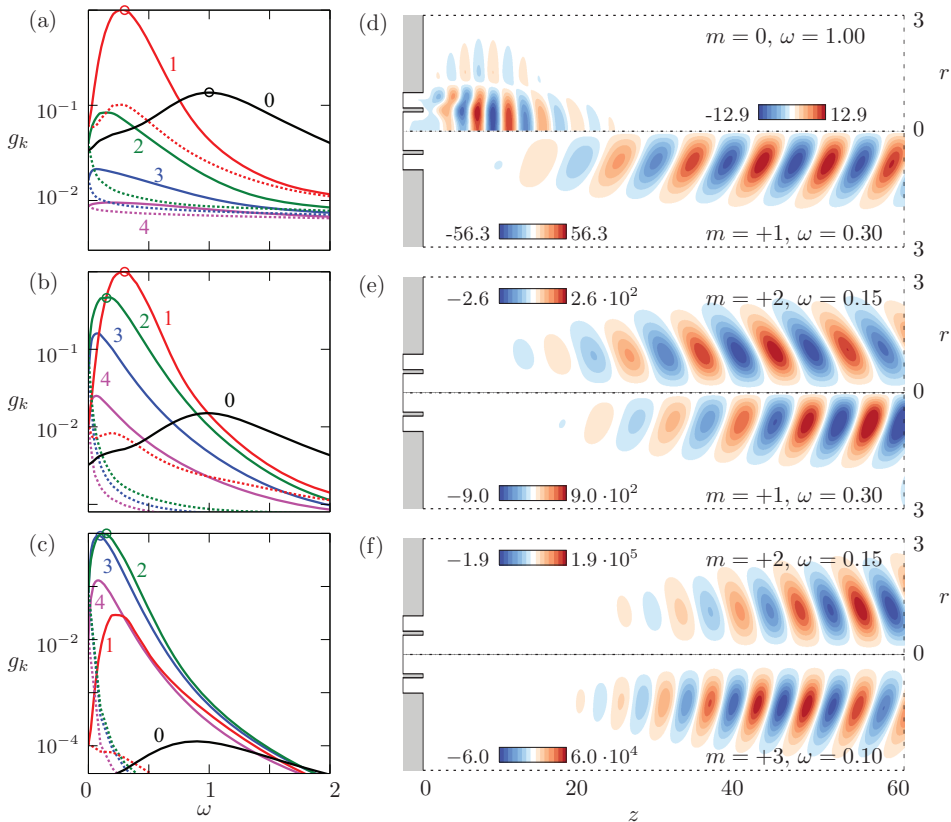
Figure 10: Influence of the swirl parameter S on the harmonic response of coaxial jets with unitary axial velocity ratio $r_u = 1$ and Re = 200. Relative contributions of the wavenumbers in the harmonic response (left) and real part of the axial velocity $\hat{u}_z$ of the preferred response (right): $S = 0.2$ (a,d); $S = 0.5$ (b,e); $S = 1.0$ (c,f). Solid lines: counter-winding structures with $m \geqslant 0$; dotted lines: co-winding structures with $m < 0$.

amplitude increases by more than an order of magnitude. For the axisymmetric mode the increase seems a bit larger. This fact may in part explain why, for higher Reynolds numbers, the axisymmetric mode dominates the flow dynamics near the nozzle (Dahm *et al.* 1992). This behaviour is slightly different when a velocity ratio $r_u = 2$ is considered, figure 12(a) to be compared with figure 8(a), with a slightly stronger increase in the amplitude of the response of the azimuthal wavenumbers $m = \pm 1, \pm 2$ and ± 3 with respect to the axisymmetric perturbations. When a swirl is present, the picture changes dramatically. From figure 11(c) it is apparent that the responses of perturbations with higher wavenumbers, $m = +2, +3, +4$, increase most with the Reynolds number, so that they become dominant over the response for $m = +1$. The increase in the amplitude is also notable: more than three orders of magnitude by just doubling the Reynolds numbers. The amplification of the most amplified modes is very similar, so that it is hard to predict which wavenumber will be selected in the actual flow. A nonlinear analysis as in (Mantič-Lugo & Gallaire 2016) seems to be necessary to answer this question, but it is out of the scope of the present work.
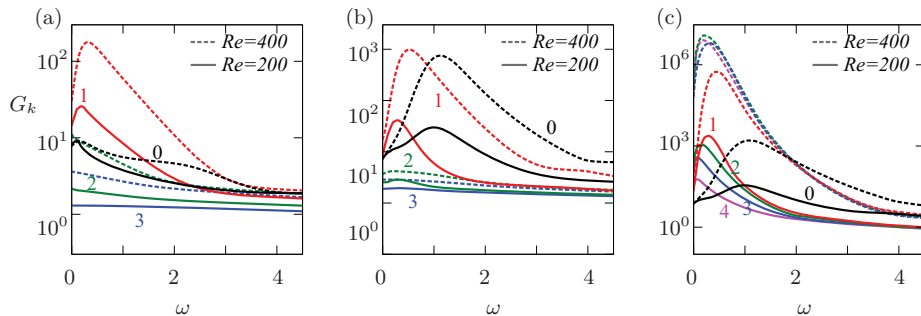
Figure 11: Influence of the Reynolds number Re on the harmonic response of three configurations of the system: (a) single jet; (b) non-swirling coaxial jets with unitary velocity ratio; (c) coaxial jets with unitary velocity ratio and swirl parameter $S = 0.5$. Solid lines: Re = 200; dotted lines: Re = 400. Colours as in the caption of figure 9.
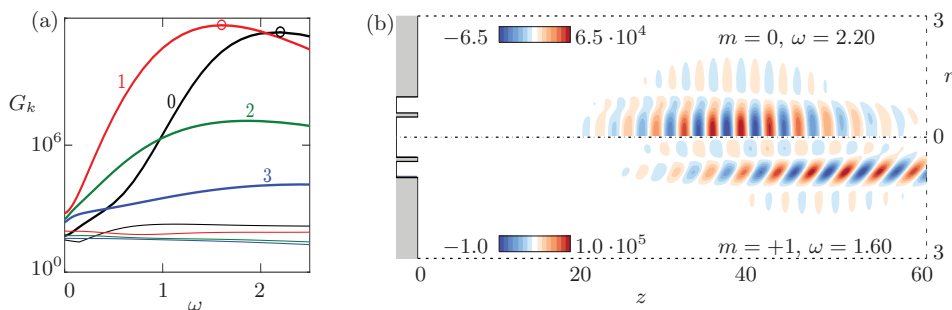

Figure 12: Harmonic response for $(\mathrm{Re}, r_u, S) = (400, 2.0, 0.0)$. (a) Relative contributions of the wavenumbers. Thick lines indicate the optimal harmonic gain, while thin lines the first suboptimal harmonic gain. The small circles on the curves correspond to the preferred response shown in the right frame. (b) Real part of the axial velocity $\hat{u}_z$ of the preferred response.

It is also interesting to compare the change induced by an increase in the Reynolds number in the shape of the optimal response. This is possible by looking at figure 12(b) and 8(b). From the figures, it is apparent that increasing the Reynolds number moves the maximum of the amplitude farther from the nozzle. For $m = \pm 1$ there is also a change in the shape of the response. The maximum response concentrates in the outer jet, with non-negligible contributions coming from the inner jet and from the outer region.

6. Nonlinear simulations

The validity of the assumptions made, the results of the harmonic response and the predominance of the harmonic response of the perturbed system are assessed by means of three-dimensional, nonlinear time simulations. All the flows analysed in this chapter are globally stable but behave as noise amplifiers: no self-sustained oscillations are observed in the system with nominal boundary conditions, namely a flow supplied with the steady boundary conditions that were used to compute the base flow, see §2. The situation may

change dramatically when perturbations are present. As a matter of fact, the strong amplification of the disturbances at the inflow, that inevitably characterise experiments, may result in substantial deviation of the flow from its stable base state. Therefore, a random disturbance, uncorrelated in both time and space and among the velocity components, has been added to the nominal boundary conditions. The disturbance has a maximum amplitude of 2.5% of the reference velocity and it is uniformly distributed in the interval $(-0.025\widetilde{U}_a, 0.025\widetilde{U}_a)$. While the assumption that disturbances can be well represented by a band-limited white noise may seem crude, two observations are in order: the actual noise in an experiment or in a real device can hardly be fully characterised, especially when complex nozzle geometries are concerned as in swirled burners. Vorticity in the wake of internal obstacles, acoustic and thermal perturbations and incoming turbulence can all be causes of inlet perturbations. Moreover, the stochastic response analysis relying on the harmonic response analysis usually assumes a white noise as input. As a matter of fact, it is generally recognised that a white noise can be considered a sufficiently general and accurate approximation to investigate the jet behaviour in an experimental environment (Cohen & Wygnanski 1987; Gohil *et al.* 2012; Balarac *et al.* 2007; Jeun *et al.* 2016). This assumption is also exploited in recent works on the prediction of large coherent structures, which characterise the early development of turbulent jets, carried out by a resolvent analysis similar to the present one applied to the mean flow, obtained either experimentally (Semeraro *et al.* 2016; Lesshafft *et al.* 2018) or numerically (Schmidt *et al.* 2018). The very good matching between the coherent structures educed by linear resolvent analysis and those extracted from the experiments and nonlinear simulations testifies for the applicability of the assumption. The introduction of perturbations is meant to investigate the relevance of the results of the linear input–output analysis in predicting the nonlinear dynamics of real coaxial jets. The amplitude of the perturbations has been chosen sufficiently high to make the amplified perturbations significant in a sufficiently short distance from the nozzle for the low Reynolds numbers investigated here, even if, from the viewpoint of a laboratory experiment, they can be considered quite high. The adopted amplitude is actually slightly less than that used by Balarac *et al.* (2007) in their DNSs at Re = 3000.

6.1. *Coaxial jets* $(\mathrm{Re}, r_u, S) = (200, 2.0, 0.0)$

We begin with a non-swirled jet with velocity ratio $r_u = 2$. Starting the simulation from the globally stable base flow, the transient growth of quite a coherent structure is observed after the noise is turned on: an axisymmetric perturbation grows in the domain while it is convected downstream. When this initial perturbation is convected out of the domain and the initial transient is over, clear dynamics appear: axisymmetric oscillations, in the form of annular vortices, with a frequency $\omega \approx 2.0$ develop in the upstream part of the domain; these annular perturbations tilt and a sinuous structure arises in the second half of the domain, whose frequency is half of the original one.

The Koopman mode analysis is used here to obtain a better insight in the dynamics of the perturbed jet. A sequence of $n = 96$ snapshots $\mathsf{U}_0^n = \{\boldsymbol{u}_i\}_{i=0}^n = \{\boldsymbol{u}(t_0 + i\Delta t)\}_{i=0}^n$, sampled every $\Delta t = 0.2$ time units, is used in the analysis to identify the structures associated with the two main frequencies. The corresponding sampling frequency is largely sufficient to capture all the amplified perturbations. Sampling starts at $t_0 = 200.0$ in order to exclude the transient behaviour. All the Koopman values lie on the unit circle in the complex plane, i.e. $|\lambda_j| = 1.0$, indicating that the system evolves on an attracting set (Rowley *et al.* 2009), see figure 13(a). The two prevailing modes oscillate with circular frequencies $\omega_1 = \angle\lambda_1/\Delta t = 0.98$ and $\omega_2 = 1.97$: these values are very close to the pseudo-resonance peaks in the harmonic response of the sinuous mode $\hat{\boldsymbol{u}}_1(\omega)$ with wavenumber
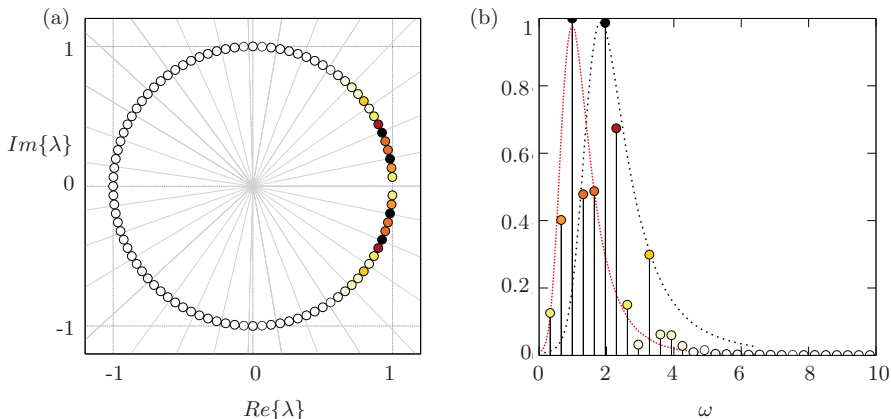
Figure 13: Koopman analysis of the flow for $(\mathrm{Re}, r_u, S) = (200, 2.0, 0.0)$. (a) Koopman values λ_j in the complex plane: two consecutive light grey radii enclose a circular sector spanning $\Delta\omega = 1.0$. The marker colour varies from white to black according to the mode amplitudes, as defined in the right figure; (b) Normalised amplitudes of the Koopman modes. Thin loosely and densely dotted lines represent the optimal harmonic gains of the axisymmetric and sinuous mode respectively.

$m = 1$ and the axisymmetric mode $\hat{\boldsymbol{u}}_0(\omega)$. Only positive frequencies are shown in figure 13(b), since the Koopman values and modes come in complex conjugate pairs. The first Koopman mode, oscillating at ω_1, is associated with the low-frequency sinuous structure arising in the downstream portion of the domain, see figure 14(a): this structure closely resembles the optimal harmonic response $\hat{\boldsymbol{u}}_1(1.0)$ close to the pseudo-resonant peak shown in figure 14(b). The second Koopman mode, oscillating at ω_2, is associated with the axisymmetric perturbations observed close to the nozzle whose contour levels are depicted in figure 15(a): the axisymmetric structure grows in the upstream part of the domain before starting to decay and lose its symmetry, and being eclipsed by the sinuous structure further downstream. This Koopman mode clearly resembles the axisymmetric preferred response $\hat{\boldsymbol{u}}_0(2.0)$ in the upstream portion of the domain depicted in figure 15(b). These observations suggest that the evolution of these modes is almost independent from each other, for such a low Reynolds number and amplitude, with the linear receptivity of the flow being responsible for selecting, by linear amplification, the dominating dynamics in each region of the flow. Apparently, the nonlinear interaction between the two most amplified modes does not play a role, for the present value of the parameters. Therefore, the linear analysis is sufficient to draw a clear picture of the flow behaviour in this case. It is interesting to note that the spatial structure of the modes plays an important role, not only their amplification. Indeed, the axisymmetric mode is dominant upstream while the sinuous mode with $m = \pm 1$ is dominant downstream, exactly as anticipated by the linear input-output analysis.

6.2. Coaxial jets $(\mathrm{Re}, r_u, S) = (400, 2.0, 0.0)$

As explained in §5, the amplification of the incoming disturbances rapidly grows with the Reynolds number. It is therefore interesting to investigate the impact of an increased Reynolds number on the fate of inlet perturbations. For this purpose, we run a DNS for a non-swirling jet with $r_u = 2$ as before, but with doubled Reynolds number, $\mathrm{Re} = 400$. The random perturbations have the same properties as in the previous case. While two
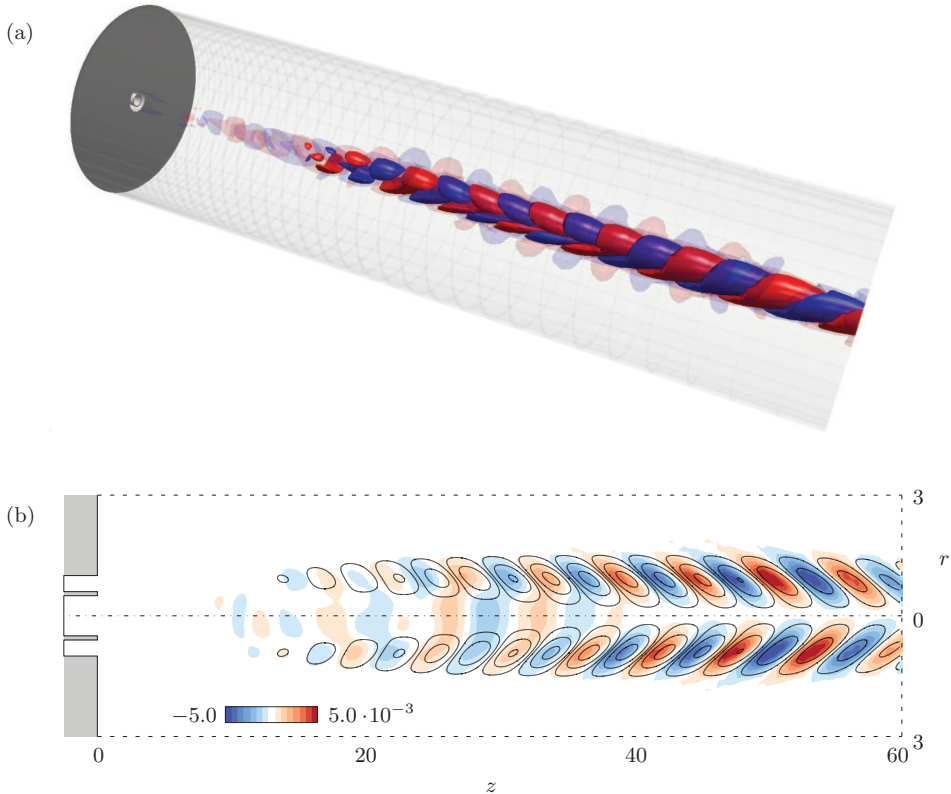
Figure 14: Koopman mode 1 (sinuous) for the flow with $(\mathrm{Re}, r_u, S) = (200, 2.0, 0.0)$. (a) Real part of the axial velocity: contour levels corresponding to 15% (opaque) and 2% (transparent) of the maximum value in the domain. (b) Contour lines of the axial velocity of the optimal harmonic response for $m = +1$, $\omega = 1.0$ superimposed on a slice of the first Koopman mode.

coherent oscillating structures, that behave almost independently from each other, have been observed in the previous section for $\mathrm{Re} = 200$, velocity perturbations at the inflow promote the transition to a turbulent regime in the globally stable flow for $Re = 400$, see figure 16. As happened for the lower Reynolds number, also in this case the varicose mode obtained by the optimal harmonic response prevails in the upstream part of the domain, for $z < 20$. This is expected, since the varicose mode dominates the linear response in the region closer to the nozzle. The varicose mode appears as a train of axisymmetric vortices that arise owing to a Kelvin-Helmholtz instability of the shear layers formed by the outer jet. After a few jet diameters from the nozzle, the vortices start interacting nonlinearly, rolling up and pairing, and are finally subject to a three-dimensional instability

The Koopman analysis of the entire flow field highlights the prevalent low-frequency broad-band dynamics of the turbulent region, as reported in figure 16(e-f). The spectrum is almost monotonically decaying with the frequency, figure 16(e), while the dominating Koopman modes reported in figure 16(f) show a highly irregular pattern and the linear spreading typical of the turbulent jet (Balarac & Métais 2005). Since, in the Koopman analysis, the dynamics in the turbulent region stand above the coherent oscillations
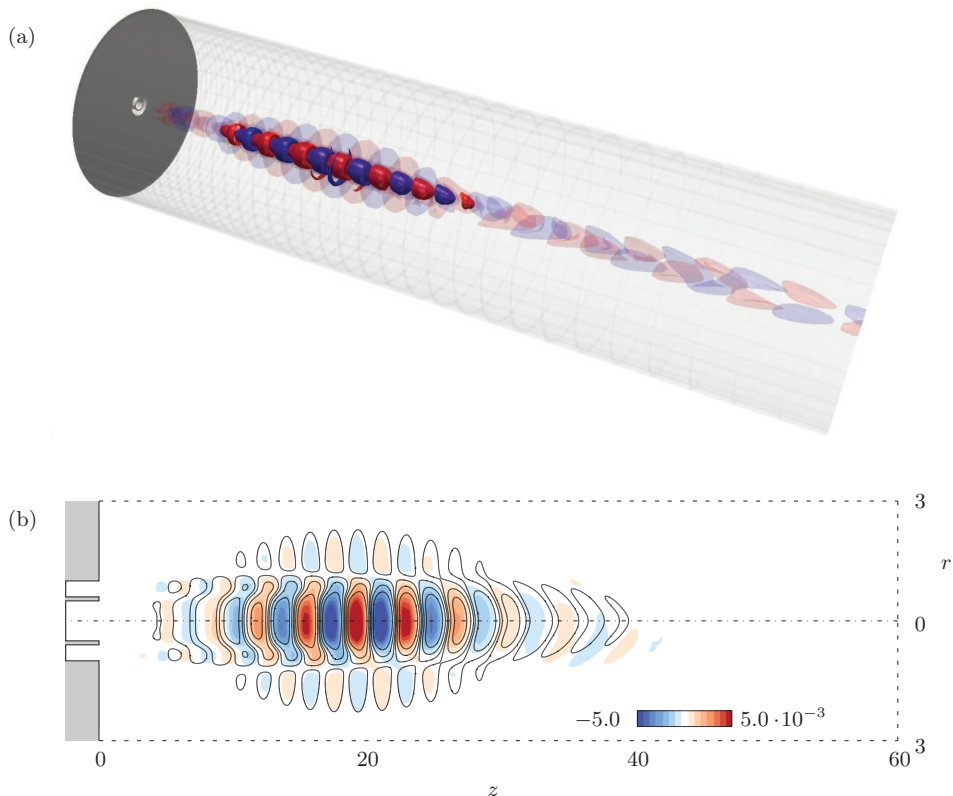
Figure 15: Koopman mode 2 (varicose) for the flow with $(\mathrm{Re}, r_u, S) = (200, 2.0, 0.0)$. (a) Real part of the axial velocity: contour levels corresponding to 15% (opaque) and 2% (transparent) of the maximum value in the domain. (b) Contour lines of the axial velocity of the optimal harmonic response for $m = 0$, $\omega = 2.0$ superimposed on a slice of the second Koopman mode.

of the jet close to the nozzle, the laminar and transitional flow in the initial part of the jet is examined by analysing the flow field on a truncated domain for $z < z_{\mathrm{DMD}}$. After a cut-off coordinate z_{DMD} is chosen, the *observable* is defined as the restriction of the velocity field to the truncated domain. Two different truncated domains have been analysed, with different lengths: $z_{\mathrm{DMD}} = 20$, that represent approximately the location where the amplitude of the response in the nonlinear simulation is small, and $z_{\mathrm{DMD}} = 25$, that represents the approximate maximum axial coordinate for which an ordered flow is observed in the simulation. The comparison of figures 16 (b), (d) and (f) shows clearly that the amplitude of the Koopman modes grows with the length of the truncated domain, from this observation we infer that the amplitude of the response keeps growing until the flow becomes turbulent.

Let us consider the Koopman analysis carried out in the shortest domain, namely for $z_{\mathrm{DMD}} = 20$. The frequency–amplitude plot reported in figure 16(a) clearly shows two peaks. One, has a frequency $\omega = 2.4$ that matches quite closely the most amplified axisymmetric forcing at the inlet, $\omega_0 = 2.2$. The second one has a frequency $\omega = 3.9$ that does not correspond to any of the peaks of harmonic gain for the tested azimuthal

wavenumbers m. On this point, it is interesting to analyse the most amplified mode at the truncation threshold. In this case we have a circular frequency slightly larger than 2.2 for the axisymmetric response, while $\omega_{\pm 1} \approx 2.2$. It must be said that the amplification of the axisymmetric mode is approximately one order of magnitude larger than that of the sinuous mode for this abscissa. This is probably the reason why the sinuous mode, that can reach an amplification factor two orders of magnitude larger further downstream, does not dominate over the axisymmetric mode in the present results. The fact that axisymmetric perturbations are most amplified in this region explains the basically axisymmetric character of the dominant Koopman modes reported in figure 16(b). Actually, the higher frequency peak observed in figure 16(a) corresponds to that of most amplified mode for a shorter truncation, $z_{\mathrm{DMD}} = 8$, not shown here for conciseness. The persistence of such a peak for longer distances from the nozzle could be related to nonlinear selection effects.

For $z > 20$, the flow strongly departs from axial symmetry. A detailed analysis of the transition process is out of the scope of the present work, but we just observe that, as a result of the interaction of the oscillations in the high-velocity annular region, a predominant transitional mode emerges with $\omega = 1.3$, figure 16(c,d), significantly lower than that of the aforementioned dominant linear modes. This fact is not surprising, since the nonlinear vortex roll-up and pairing may lead to a significant decrease of the peak frequency in the spectrum.

A question arises about which, of the dominant modes observed for $z_{\mathrm{DMD}} = 20$, dominates the transition process, since in the linear analysis there is no evidence of the dominance of one mode over another. To investigate this point, we ran simulations where we forced the jet with the optimal inlet forcing with $m = 0$ and $m = +1$ resulting from the optimal harmonic gain analysis described in the previous section, see figure 17. The simulations show that the dynamics of the jet forced with $m = 0$ lead to transition by the process of vortex roll-up, vortex pairing and instability of the vorticity braid connecting two adjacent vortices that produces outward ejections and quickly leads to transition to turbulence, as described for the single jet in (Brancher *et al.* 1994) and (Liepmann & Gharib 1992). A different process is observed when the jet is forced with $m = +1$. In this case, a sinuous mode prevails similar to that observed in swirling jets and leading to vortex breakdown. The jet becomes turbulent just after the core of the jet shows a marked helical shape. By comparing the nonlinear response of two jets forced with the same amplitude, it can be observed that the transition process is significantly faster in the second case, namely when the jet is forced with $m = +1$. While this observation does not answer to the previous question, it seems to indicate that for this value of the parameters, the effectiveness of the two forcing modes in producing transition to turbulence is not equivalent, with the $m = \pm 1$ inlet forcing, the most amplified according to the linear analysis, being more effective.

6.3. *Swirling coaxial jets* $(\mathrm{Re}, r_u, S) = (200, 1.0, 1.0)$

We now investigate the impact of a swirling outer jet on the behaviour of the flow in the nonlinear regime. A DNS of the coaxial jets with unit axial velocity ratio $r_u = 1.0$ and swirling outer stream with $S = 1.0$ shows a non-trivial combination of structures with different azimuthal wavenumbers. This behaviour was somehow expected, since the amplitude of the linear response depicted in figure 10(c) shows that several modes with different wavenumbers enjoy a strong amplification, those with $m = +2$ and $m = +3$ being the most amplified ones.

To better understand the flow behaviour, we sliced the velocity field with a plane normal to the axial direction and analysed the velocity field in such a plane. The axial
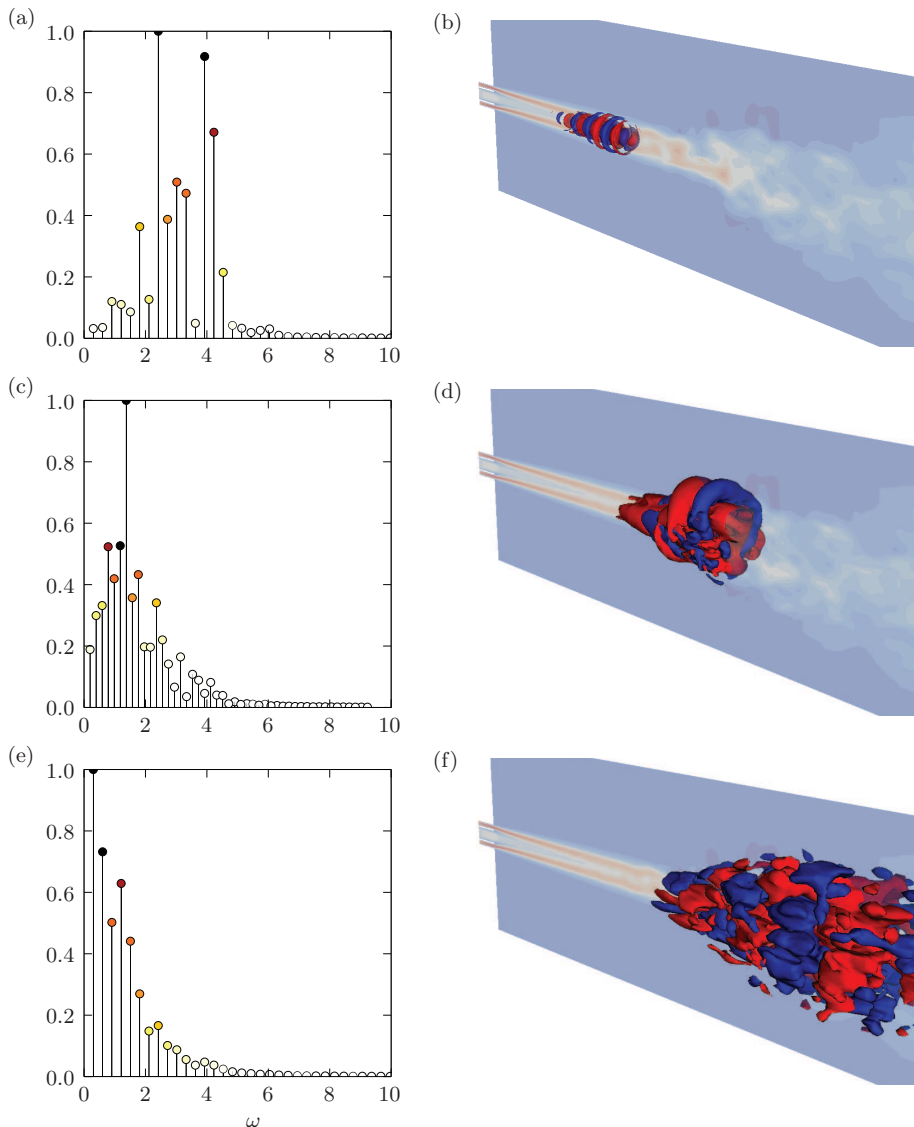
Figure 16: Coaxial jets with $(\mathrm{Re}, r_u, S) = (400, 2.0, 0.0)$. DMD analysis of nonlinear time simulations: spectra and prevalent Koopman modes. (a-b) $z_{\mathrm{DMD}} = 20$, (c-d) $z_{\mathrm{DMD}} = 25$, (e-f) $z_{\mathrm{DMD}} = L_c = 60$.

velocity field on the slice $\Omega_{\bar{z}}$, with $\bar{z} = 35.0$ unit lengths far from the nozzle, is shown in figure 18(a): the prevalence of a structure with azimuthal wavenumber $m = +3$ becomes evident in figure 18(b) when the velocity field is purged from the axisymmetric contribution. This behaviour can be interpreted by looking at figure 10(c) and (f). From figure 10(c), it is clear that the two modes with $m = +2$ and $m = +3$ are dominant, with the former slightly prevailing over the latter. Figure 10(f), however, shows that the mode $m = +3$ reaches its maximum for a distance from the nozzle lower than that of the mode $m = +2$, so that it not surprising that its contribution dominates for $\bar{z} = 35.0$. This slice of the velocity field is analysed by Fourier series in the azimuthal coordinate
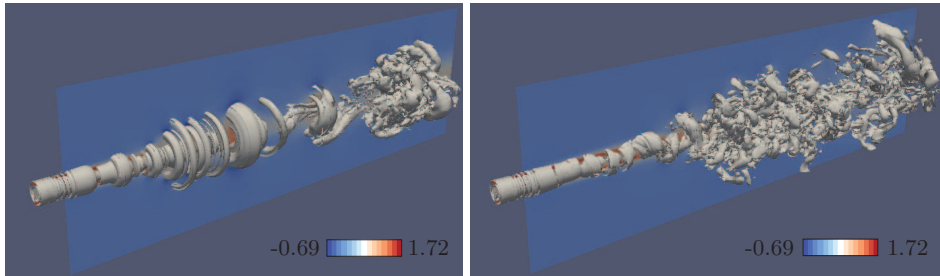
Figure 17: Nonlinear response of the coaxial jet to optimal forcing with wavenumber $m = 0$, left, and $m = 1$, right, for $(\mathrm{Re}, r_u, S) = (400, 2.0, 0.0)$. The Q criterion is used to visualise the vortical structures in 3D in both cases. The color map corresponds to the axial velocity component in a radial plane.

θ,

$$\boldsymbol{u}(r, \theta, \overline{z}, \overline{t}) = \sum_{m=-\infty}^{\infty} \tilde{\boldsymbol{u}}_m(r, \overline{z}, \overline{t}) e^{im\theta} = \sum_{m=0}^{\infty} \boldsymbol{u}_m(r, \theta, \overline{z}, \overline{t}), \tag{6.1}$$

in order to obtain a more detailed information about the wavenumber contributions. It is worthwhile to note that the discretisation of the transverse slice in $N_\theta = 60$ circular sectors implies that the series is truncated to $|m| \leqslant N_\theta/2$. The real contribution $\boldsymbol{u}_m = 2\,\mathrm{re}\left\{\tilde{\boldsymbol{u}}_m e^{im\theta}\right\}$ of the lower positive wavenumbers is depicted in figure 18(d-f): more than 97% of the L^2-norm of the non-axisymmetric part of the field comes from the first three modes, see (c), and the contribution of the fourth mode is approximately 1.7%.

The time average of the L^2-norm of the velocity field,

$$A_m = \frac{1}{T} \int_{t_i}^{t_i+T} \|\boldsymbol{u}_m\|_{L^2(\Omega_z)}, \tag{6.2}$$

is used in figure 19(a-c) to evaluate the relative shares of the modes on three different sections of the domain. The initial time t_i is set to 300 in order to exclude the transient behaviour and T is set to 300 as well. While energy is almost evenly distributed among the first three modes at $z = 15.0$, the second and the third modes prevail downstream along the domain (b,c). Higher wavenumbers have little contributions only in terms of energy. Figure 19(d) shows the temporal evolution of the integral quantity

$$I(\theta, t) = \int_0^R |\boldsymbol{u}(r, \theta, \overline{z}, t)|\, r\, dr. \tag{6.3}$$

This function exhibits quite a regular pattern in the $\theta - t$ plane, because of the interference of the dominant modes with $m = +2$ and $m = +3$. Local extrema of the function $I(\theta)$ emerge from the local extrema of the prevailing modes, whose phase velocity is almost constant in time. A constant approximation of the phase velocity of the modes is obtained as the slope of the linear fit of the "characteristic lines" describing the azimuthal coordinates of the maximum values of $I_m(\theta)$ as a function of time, being $I_m(\theta)$ the integral quantity obtained from the m-th mode. Interference occurs as a result of the combination of modes with different phase velocity and the regular pattern in figure 19(d) lies on the frame described by the characteristic lines associated with the prevailing modes. The constant approximation of the phase velocity $\Omega = \Delta\theta/\Delta t$ leads to $\Omega_2 = -0.078$ and $\Omega_3 = -0.032$ for $\boldsymbol{u}_2$ and $\boldsymbol{u}_3$ respectively. These values are close
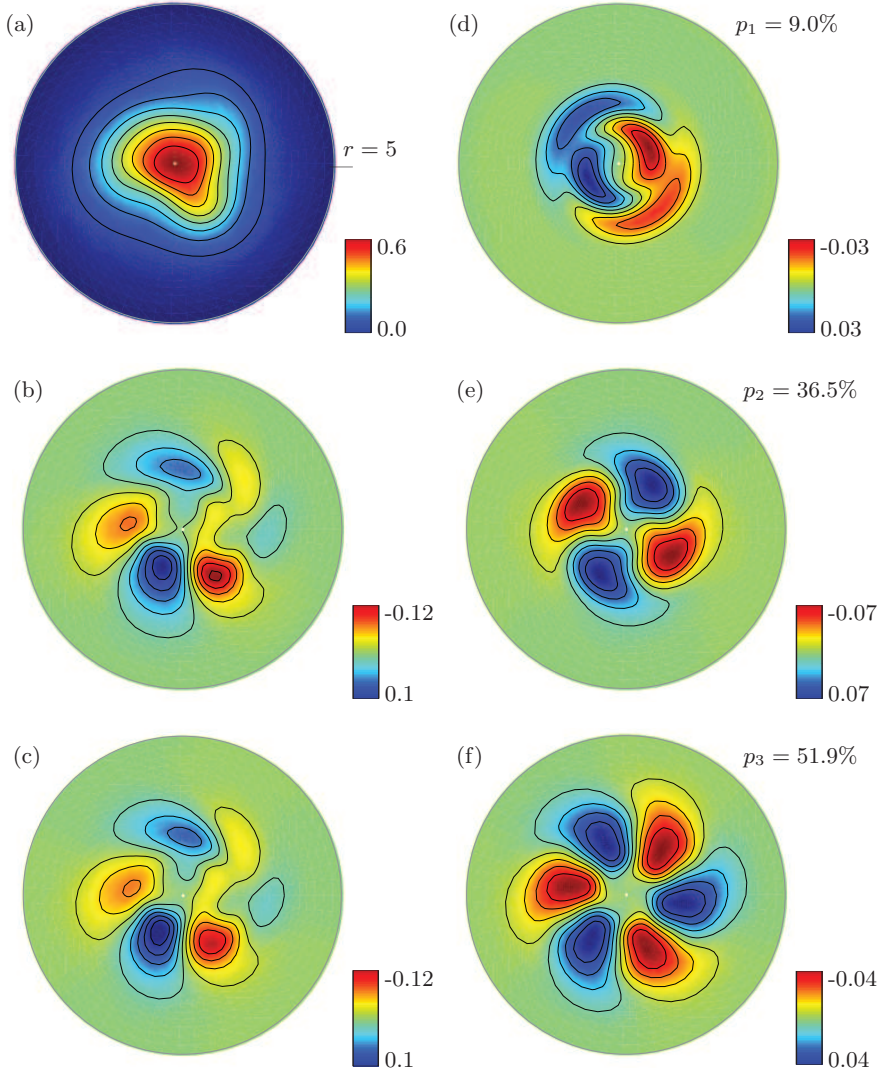
Figure 18: Coaxial jets for $(\mathrm{Re}, r_u, S) = (200, 1.0, 1.0)$. Axial component $u_z(r, \theta, \overline{z}, \overline{t})$ of the velocity field on the transverse section $\overline{z} = 35.0$. (a) Field at time $\overline{t} = 490.0$; (b) non-axisymmetric part of the field, $u_z - u_{z,0}$; (d-f) non-axisymmetric real modes $u_{z,1}$, $u_{z,2}$, $u_{z,3}$, whose contribution $\sum_{k=1}^{3} u_{z,k}$ is shown in figure (c). The relative contribution of a mode to the complete field is defined as the ratio of L^2-norms, $p_m = \|\boldsymbol{u}_m\|_{L^2(\Omega_{\overline{z}})}/\|\boldsymbol{u}\|_{L^2(\Omega_{\overline{z}})}$. In contrast to what done in previous figures, black contours are used in this figure only to increase the readability of the colour map.

to the phase velocity of the pseudo-resonant harmonic perturbations shown in figure 9(b), $-\overline{\omega}_2/2 = -0.083$ and $-\overline{\omega}_3/3 = -0.034$. This result confirms the relevance of the linear input-output analysis to predict, not only qualitatively but also quantitatively, the behaviour of absolutely-stable, but convectively unstable, developing flows.
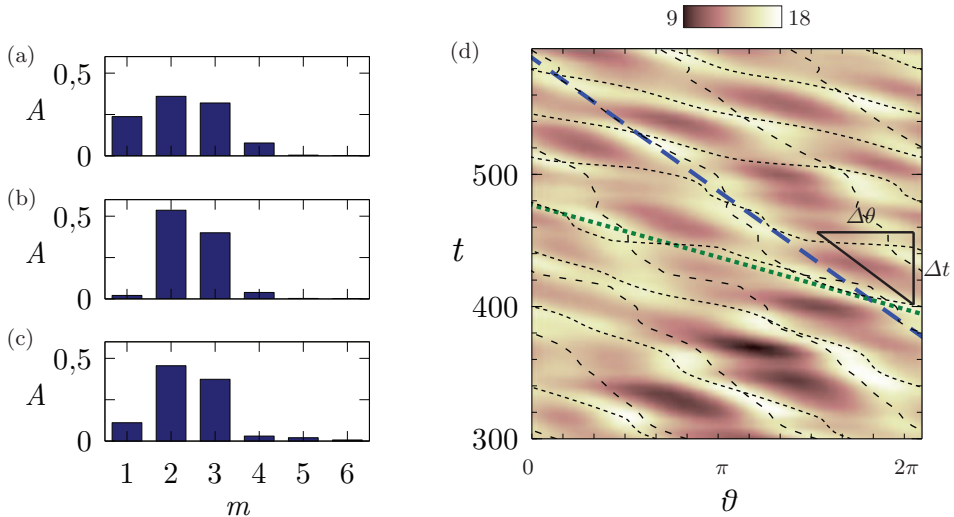
Figure 19: Coaxial jets for $(\mathrm{Re}, r_u, S) = (200, 1.0, 1.0)$. Time-averaged mode contributions as functions of the axial coordinate z, (a) $z = 15.0$, (b) $z = 25.0$, (c) $z = 35.0$, and (d) time evolution of the field $I(\theta)$ on $\Omega_{\bar{z}}$: green dotted line and blue dashed line are the best linear fit of the black lines representing the evolution of the coordinate θ of the maximum of the modes with $m = +2$ and $m = +3$, respectively. The slope of these lines represents the average value of the phase velocity $\omega = \Delta\theta/\Delta t$ of the corresponding mode.

7. Conclusions

In this work, we present the first published investigation dealing with the convective stability of swirling coaxial jets to both axisymmetric and non-axisymmetric perturbations in a global framework. In particular, the response of coaxial jets to external forcing at the inlet is investigated for subcritical Reynolds numbers. Three parameters identify the coaxial jets considered here: the Reynolds number Re, which is defined here in terms of the velocity and diameter of the inner jet, the outer-to-inner axial velocity ratio r_u and the swirl number S of the outer stream. Their effects on the response of the system have been assessed by means of non-modal analysis in the frequency domain.

The main new findings provided by the present work can be summarised as follows: i. In non-swirling coaxial jets, two axisymmetric modes, corresponding to two local maxima in the harmonic response, swap their role as most amplified mode when the velocity ratio is increased over 0.75. This swap explains the importance of the axisymmetric mode observed experimentally for high velocity ratios, since the dominant mode for high Reynolds number is quite concentrated in the region near the nozzle. ii. In non-swirling coaxial jets, the axisymmetric $m = 0$ and sinuous $m = \pm 1$ modes compete as mostly amplified modes for high velocity ratios. This competition can lead to different forms of transition, depending on which component dominates the inlet perturbation. iii. In swirling jets, azimuthal wavenumbers higher than $m = +1$ are progressively dominant, as the swirl number is increased. iv. The amplification of inlet perturbations is dominated by the Kelvin–Helmholtz instability for swirling coaxial jets, while centrifugal instabilities are relatively unimportant in the portion of the parameter space investigated here. v. For the lower Reynolds number tested here, the results of the linear harmonic-gain analysis are very successful in predicting the nonlinear flow behaviour, while doubling

the Reynolds number the indications of linear analysis are less effective in predicting the flow behaviour.

To be more precise, our results show that non-swirling jets are dominated by the response at lowest wavenumbers, with $m = 0$ and $m = \pm 1$, with the relative amplitude of the dominant modes, and the spatial structure of the response, changing with the velocity ratio r_u. In particular, the axisymmetric mode, which is subdominant for low r_u, becomes more and more important for $r_u \geqslant 1$ and has a spatial structure very different from that of the sinuous $m = \pm 1$ modes, being stronger than the latter in the region near the nozzle. This result agrees well with both experimental and numerical simulations reported in the literature.

The rotation of the outer stream has destabilising effects on the globally stable columnar flow. Counter-winding modes are the most amplified, suggesting that the amplification mechanism may be associated with a Kelvin–Helmholtz instability and not with a centrifugal instability. The response amplitude of intermediate wavenumbers $m = +2, +3, +4$ grows exponentially fast with the swirl parameter for $0.5 \leqslant S \leqslant 1$. The harmonic response of the system involves structures with larger azimuthal wavenumbers whose amplification grows exponentially with S leading to the helical responses with $m = +2$ and $m = +3$ being dominant for the highest swirl numbers investigated. The spatial structure of the response is similar for the dominant modes, with the maximum peak being located quite far from the nozzle. The Reynolds number is mainly related with the amplitude of the response for non-swirling flows. When swirl is present, the intermediate wavenumbers seem more affected, so that the hierarchy of the amplification can change with the Reynolds number.

Direct numerical simulations confirm the absolute stability of the unperturbed flow, with initial perturbations being washed out of the computational domain and the flow approaching asymptotically the steady baseflow computed for the linear stability calculations. To mimic experiments, direct numerical simulations of the flow perturbed at the inlet with a small spatially and temporally uncorrelated white noise distribution have been performed for two different Reynolds numbers, $\mathrm{Re} = 200$ and 400, for a non-swirling flow with $r_u = 1$, and for $\mathrm{Re} = 200$, $r_u = 1$ and $S = 1$. A Koopman analysis has been used to obtain a better insight in the flow behaviour of the non-swirling jets. For the lowest Reynolds number, the analysis shows that the nonlinear response matches almost perfectly that predicted by the linear analysis. For the highest Reynolds number, the response in the region close to the nozzle, say for $z < 20$, retains some properties that can be related to the linear response of the flow, while further downstream of this region nonlinear effects become more and more important and rapidly lead to transition to turbulence. This result seems important as it underlines, at least in the present case, the effectiveness of the linear analysis in predicting the early phases of the transition process. The present analysis shows that for spatially developing flows as jets, both the amplitude and the spatial structure of the harmonic response play an important role in predicting the actual response of the disturbed system. The good predictive capability of the linear analysis is confirmed also when a swirl motion is added to the flow. The Fourier analysis of some slices of the velocity fields obtained by means of nonlinear simulations shows prevailing modes whose wavenumber and phase velocity correspond well with the results of the frequency response of the linearised system. However, in the nonlinear regime, for the higher Reynolds number investigated here, we found the flow sensitive to the actual shape and amplitude of the perturbation. The reason is probably related to the fact that competing transition mechanisms can become effective, depending on the properties of the perturbation, especially when the Reynolds number is high and the amplification

Mesh	N_e	N_{dof}
M_1	193414	1265763
M_2	259744	1698847
M_3	331824	2168781

Table 2: Meshes used for the grid sensitivity analysis. N_e number of triangular elements. N_{dof} number of degrees of freedom for the $\mathbb{P}_2$ approximation of three-dimensional velocity field and the $\mathbb{P}_1$ approximation of the pressure field.
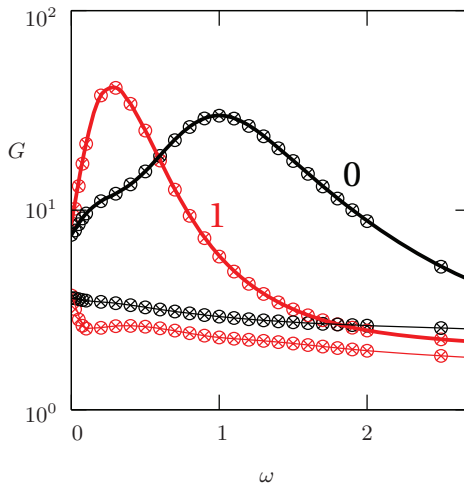

Figure 20: Grid sensitivity for $(\mathrm{Re}, r_u, S) = (200.0, 1.0, 0.0)$. Optimal (thick) and first sub-optimal (thin) gains for varicose and sinuous response: M_1 (circles), M_2 (crosses), M_3 (spline interpolation).

of the perturbations becomes very strong. Further studies seem to be necessary to fully understand the transition process in coaxial jets.

Appendix A. Grid sensitivity

Mesh independence of the results obtained in this work has been checked. The numerical domain used for non-modal analysis has the same axial extension $L_c = 60$ as the numerical domain used by Canton *et al.* (2017) for the modal analysis. The radial extension of the domain is set to $R_c = 8$. Figure 20(a) shows the results of the non-modal harmonic analysis of the coaxial jets for $(\mathrm{Re}, r_u, S) = (200, 1, 0)$ carried out on the meshes listed in table 2. The harmonic gains computed on the coarser meshes match the corresponding gains obtained on the most refined mesh M_3, over the whole range of frequencies examined. The maximum amplification of the axisymmetric and sinuous modes computed using meshes M_1 and M_2 differs less than 0.4% and 0.01% from the values obtained using mesh M_3, respectively.

The independence of the results with respect to the domain extent has also been checked. In particular, we checked that the shape of the optimal response is not affected
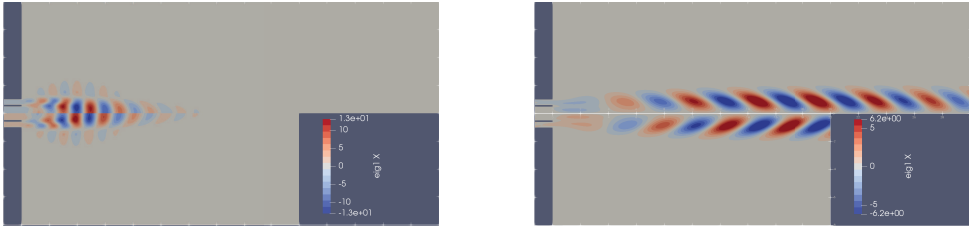
Figure 21: Optimal linear response of the coaxial jet to optimal forcing with wavenumber $m = 0$ and $\omega = 1.0$, left, $m = 1$ and $\omega = 0.3$, right, for $(\mathrm{Re}, r_u, S) = (200, 1.0, 0.0)$. The top of the two frames represent the results for a domain length of 30 inner diameters, the bottom ones for a domain length of 20 inner diameters.

by an extension of the domain, as reported in figure 21. The same is not true for the gain value when the harmonic response extends very far from the nozzle, as for instance when swirl is present, since the gain is computed using the classic L^2 norm. In this case, reaching domain independence would require extremely long domains with limited added value, since the most interesting flow phenomena take place in a region not too far from the nozzle. On this point it is worthwhile to notice that, as pointed out by Garnaud *et al.* (2013*b*), the choice of the most suitable norm for computing the harmonic gains is still an open question. Our results suggest, in particular, that the region near the nozzle becomes more and more important as the Reynolds number is increased, but a deeper investigation will be necessary to answer the question on which the best norm would be to use in the linear harmonic gain analysis to investigate transition.

REFERENCES

BALARAC, G. & MÉTAIS, O. 2005 The near field of coaxial jets: A numerical study. *Physics of Fluids* **17** (6), 065102.

BALARAC, G., MÉTAIS, O. & LESIEUR, M. 2007 Mixing enhancement in coaxial jets through inflow forcing: A numerical study. *Physics of Fluids* **19** (7), 075102.

BATCHELOR, G.K. & GILL, A.E. 1962 Analysis of the stability of axisymmetric jets. *Journal of Fluid Mechanics* **14** (4), 529–551.

BILLANT, P. & GALLAIRE, F. 2013 A unified criterion for the centrifugal instabilities of vortices and swirling jets. *Journal of Fluid Mechanics* **734**, 5–35.

BLACKBURN, H.M., BARKLEY, D. & SHERWIN, S.J. 2008*a* Convective instability and transient growth in flow over a backward-facing step. *Journal of Fluid Mechanics* **603**, 271–304.

BLACKBURN, H.M., SHERWIN, S.J. & BARKLEY, D. 2008*b* Convective instability and transient growth in steady and pulsatile stenotic flows. *Journal of Fluid Mechanics* **607**, 267–277.

BOUJO, E. & GALLAIRE, F. 2015 Sensitivity and open-loop control of stochastic response in a noise amplifier flow: the backward-facing step. *Journal of Fluid Mechanics* **762**, 361–392.

BRANCHER, P., CHOMAZ, J.M. & HUERRE, P. 1994 Direct numerical simulations of round jets: Vortex induction and side jets. *Physics of Fluids* **6** (5), 1768–1774.

BURESTI, G., TALAMELLI, A. & PETAGNA, P. 1994 Experimental characterization of the velocity field of a coaxial jet configuration. *Experimental Thermal and Fluid Science* **9** (2), 135–146.

CANTON, J., AUTERI, F. & CARINI, M. 2017 Linear global stability of two incompressible coaxial jets. *Journal of Fluid Mechanics* **824**, 886–911.

CANTWELL, C. D., BARKLEY, D. & BLACKBURN, H. M. 2010 Transient growth analysis of flow through a sudden expansion in a circular pipe. *Physics of Fluids* **22** (3), 034101.

CHAMPAGNE, F.H. & WYGNANSKI, I.J. 1971 An experimental investigation of coaxial turbulent jets. *International Journal of Heat and Mass Transfer* **14** (9), 1445–1464.

CHAMPAGNE, F. H. & KROMAT, S. 2000 Experiments on the formation of a recirculation zone in swirling coaxial jets. *Experiments in Fluids* **29** (5), 494–504.

CHOMAZ, J.-M. 2005 Global instabilities in spatially developing flows: non-normality and nonlinearity. *Annu. Rev. Fluid Mech.* **156**, 209–240.

COHEN, J. & WYGNANSKI, I. 1987 The evolution of instabilities in the axisymmetric jet. part 1. the linear growth of disturbances near the nozzle. *Journal of Fluid Mechanics* **176**, 191–219.

CRIGHTON, D.G. & GASTER, M. 1976 Stability of slowly diverging jet flow. *Journal of Fluid Mechanics* **77** (2), 397–413.

DAHM, W.J.A., FRIELER, C.E. & TRYGGVASON, G. 1992 Vortex structure and dynamics in the near field of a coaxial jet. *Journal of Fluid Mechanics* **241**, 371–402.

DANAILA, I., DUŠEK, J. & ANSELMET, F. 1997 Coherent structures in a round, spatially evolving, unforced, homogeneous jet at low reynolds numbers. *Physics of Fluids* **9** (11), 3323–3342.

DELBENDE, I. & ROSSI, M. 2005 Nonlinear evolution of a swirling jet instability. *Physics of Fluids* **17** (4), 044103.

DUSSIN, D., FOSSATI, M., GUARDONE, A. & VIGEVANO, L. 2009 Hybrid grid generation for two-dimensional high-Reynolds flows. *Computers & Fluids* **38** (10), 1863–1875.

FARRELL, B.F. & IOANNOU, P.J 1996 Generalized stability theory. Part I: Autonomous operators. *Journal of the atmospheric sciences* **53** (14), 2025–2040.

FISCHER, P. F., LOTTES, J. W. & KERKEMEIER, S. G. 2008 `nek5000` web page. http://nek5000.mcs.anl.gov.

GALLAIRE, F. & CHOMAZ, J.-M. 2003*a* Instability mechanisms in swirling flows. *Physics of Fluids* **15** (9), 2622–2639.

GALLAIRE, F. & CHOMAZ, J.-M. 2003*b* Mode selection in swirling jet experiments: a linear stability analysis. *Journal of Fluid Mechanics* **494**, 223–253.

GARNAUD, X., LESSHAFFT, L., SCHMID, P.J. & HUERRE, P. 2013*a* Modal and transient dynamics of jet flows. *Physics of Fluids* **25** (4), 044103.

GARNAUD, X., LESSHAFFT, L., SCHMID, P.J. & HUERRE, P. 2013*b* The preferred mode of incompressible jets: linear frequency response analysis. *Journal of Fluid Mechanics* **716**, 189–202.

GOHIL, T.B., SAHA, A.K. & MURALIDHAR, K. 2012 Numerical study of instability mechanisms in a circular jet at low reynolds numbers. *Computers & Fluids* **64**, 1–18.

JEUN, J., NICHOLS, J.W. & JOVANOVIČ, M.R. 2016 Input-output analysis of high-speed axisymmetric isothermal jet noise. *Physics of Fluids* **28** (4), 047101.

KHORRAMI, M.R. 1991 On the viscous modes of instability of a trailing line vortex. *Journal of Fluid Mechanics* **225**, 197–212.

LEFEBVRE, A.H. 1998 *Gas turbine combustion*. CRC press.

LEIBOVICH, S. & STEWARTSON, K. 1983 A sufficient condition for the instability of columnar vortices. *Journal of Fluid Mechanics* **126**, 335–356.

LESSHAFFT, L., SEMERARO, O., JAUNET, V., CAVALIERI, A.V. & JORDAN, P. 2018 Resolvent-based modelling of coherent wavepackets in a turbulent jet, arXiv: 1810.09340.

LIANG, H. & MAXWORTHY, T. 2005 An experimental investigation of swirling jets. *Journal of Fluid Mechanics* **525**, 115–159.

LIEPMANN, D. & GHARIB, M. 1992 The role of streamwise vorticity in the near-field entrainment of round jets. *Journal of Fluid Mechanics* **245**, 643–668.

LOISELEUX, T. & CHOMAZ, J.-M. 2003 Breaking of rotational symmetry in a swirling jet experiment. *Physics of Fluids* **15** (2), 511–523.

LOISELEUX, T., CHOMAZ, J.-M. & HUERRE, P. 1998 The effect of swirl on jets and wakes: Linear instability of the rankine vortex with axial flow. *Physics of Fluids* **10** (5), 1120–1134.

LOISELEUX, T., DELBENDE, I. & HUERRE, P. 2000 Absolute and convective instabilities of a swirling jet/wake shear layer. *Physics of Fluids* **12** (2), 375–380.

MANTIČ-LUGO, V. & GALLAIRE, F. 2016 Self-consistent model for the saturation mechanism of the response to harmonic forcing in the backward-facing step flow. *Journal of Fluid Mechanics* **793**, 777–797.

MARTIN, J.E. & MEIBURG, E. 1994 On the stability of the swirling jet shear layer. *Physics of Fluids* **6** (1), 424–426.

MARTIN, J.E. & MEIBURG, E. 1996 Nonlinear axisymmetric and three˘2010dimensional vorticity dynamics in a swirling jet model. *Physics of Fluids* **8** (7), 1917–1928.

MATTINGLY, G. E. & CHANG, C. C. 1974 Unstable waves on an axisymmetric jet column. *Journal of Fluid Mechanics* **65** (3), 541–560.

MICHALKE, A. 1999 Absolute inviscid instability of a ring jet with back-flow and swirl. *Eur. J. Mech. B/Fluids* **18** (1), 3–12.

MORRIS, P.J. 1976 The spatial viscous instability of axisymmetric jets. *Journal of Fluid Mechanics* **77**, 511–529.

ÖRLÜ, R. & ALFREDSSON, P.H. 2008 An experimental study of the near-field mixing characteristics of a swirling jet. *Flow, Turbulence and Combustion* **80** (3), 323–350.

REDDY, S.C. & HENNINGSON, D.S. 1993 Energy growth in viscous channel flows. *Journal of Fluid Mechanics* **252**, 209–238.

REHAB, H., VILLERMAUX, E. & HOPFINGER, E.J. 1997 Flow regimes of large-velocity-ratio coaxial jets. *Journal of Fluid Mechanics* **345**, 357–381.

REYNOLDS, A.J. 1962 Observations of a liquid-into-liquid jet. *Journal of Fluid Mechanics* **14** (4), 552–556.

RIBEIRO, M.M. & WHITELAW, J.H. 1980 Coaxial jets with and without swirl. *Journal of Fluid Mechanics* **96** (4), 769–795.

ROWLEY, C.W., MEZIĆ, I., BAGHERI, S., SCHLATTER, P. & HENNINGSON, D.S. 2009 Spectral analysis of nonlinear flows. *Journal of fluid mechanics* **641**, 115–127.

SADR, R. & KLEWICKI, J.C. 2003 An experimental investigation of the near-field flow development in coaxial jets. *Physics of Fluids* **15** (5), 1233–1246.

SAIKI, Y., SUZUKI, Y. & KASAGI, N. 2011 Active control of swirling coaxial jet mixing with manipulation of large-scale vortical structures. *Flow, Turbulence and Combustion* **86** (3-4), 399–418.

SCHMID, P.J. 2007 Nonmodal stability theory. *Annual Review of Fluid Mechanics* **39** (1), 129–162.

SCHMID, P.J. 2010 Dynamic mode decomposition of numerical and experimental data. *Journal of Fluid Mechanics* **656**, 5–28.

SCHMIDT, O.T., TOWNE, A., RIGAS, G., COLONIUS, T. & BRÈS, G.A. 2018 Spectral analysis of jet turbulence. *Journal of Fluid Mechanics* **855**, 953–982.

SCHUMAKER, S.A. & DRISCOLL, J.F. 2012 Mixing properties of coaxial jets with large velocity ratios and large inverse density ratios. *Physics of Fluids* **24**, 055101–1–055101–21.

SEGALINI, A. & TALAMELLI, A. 2011 Experimental analysis of dominant instabilities in coaxial jets. *Physics of fluids* **23** (2), 024103.

SEMERARO, O., JAUNET, V., JORDAN, P., CAVALIERI, A.V. & LESSHAFFT, L. 2016 Stochastic and harmonic optimal forcing in subsonic jets. In *22nd AIAA/CEAS Aeroacoustics Conference, Lyon, France*. AIAA.

DA SILVA, C.B., BALARAC, G. & MÉTAIS, O. 2003 Transition in high velocity ratio coaxial jets analysed from direct numerical simulations. *Journal of Turbulence* **4**, N24.

TALAMELLI, A. & GAVARINI, I. 2006 Linear instability characteristics of incompressible coaxial jets. *Flow, Turbulence and Combustion* **76** (3), 221–240.

TANG, S.K. & KO, N.W.M. 1994 Coherent structure interactions in an unexcited coaxial jet. *Experiments in Fluids* **17** (3), 147–157.

VILLERMAUX, E. & REHAB, H. 2000 Mixing in coaxial jets. *Journal of Fluid Mechanics* **425**, 161–185.

WELLER-CALVO, J., FONTANE, J. & JOLY, L. 2015 Mode selection in swirling coaxial jets. In *Proceedings of Sixth International Symposium on Bifurcations and Instabilities in Fluid Dynamics (BIFD 2015), 15 July 2015 - 17 July 2015 (Paris, France)*..

WELLER-CALVO, J., JOLY, L. & FONTANE, J. 2013 Stability of coaxial swirling jets. In *66th Annual Meeting of the American Physical Society's Division of Fluid Dynamics (DFD), 24 November 2013*. American Physical Society.

WICKER, R.B. & EATON, J.K. 1994 Near field of a coaxial jet with and without axial excitation. *AIAA J.* **32** (3), 542–546.

WILLIAMS, T.J., ALI, M.R.M.H. & ANDERSON, J.S. 1969 Noise and flow characteristics of coaxial jets. *Journal of Mechanical Engineering Science* **11** (2), 133–142.